CHALMERS
UNIVERSITY OF TECHNOLOGY

UNIVERSITY OF
GOTHENBURG

Master's thesis 2016

Topological Kondo effect with Majorana fermions

POORANI GNANASAMBANDAN

Chalmers University of Technology
Gothenburg, Sweden 2016

Topological Kondo effect with Majorana fermions

Supervisor: Henrik Johannesson, Correlated Systems Group, Department of Physics, Gothenburg University.
Examiner: Thilo Bauch, Quantum Device Physics Laboratory, Microtechnology and Nanoscience, Chalmers University of Technology.
Co-promoter: Michel Houssa, Materials Modelling, Department of Physics, Katholieke Universiteit Leuven.

Master's Thesis 2016
Submitted for the degree of Erasmus Mundus Master of Nanoscience and Nanotechnology
Department of Microtechnology and Nanoscience
Chalmers University of Technology
SE-412 96 Gothenburg
Telephone +46 31 772 1000

CHALMERS
UNIVERSITY OF TECHNOLOGY

UNIVERSITY OF
GOTHENBURG

KU LEUVEN

Erasmus
Mundus

Typeset in LaTeX
Gothenburg, Sweden 2016

Abstract

One-dimensional semiconducting nanowires with strong spin-orbit coupling coupled to s-wave superconductors, and exposed to external magnetic field have been predicted to support Majorana fermion bound states at its ends. The effect of spin-orbit coupling and external magnetic field is analysed by studying the energy spectrum of the wire. The appearance of unpaired Majorana fermions at the ends of a 1D spinless p-wave superconductor is studied by means of Kitaev's toy model.

The thesis is then aimed at an analysis and possible improvement of a simple model for a quantum wire realization of the topological Kondo effect [1], with particular focus on the role of the charging energy of the superconducting island. The project entails literature studies as well as independent calculations, using mainly an analytical approach (tight-binding for noninteracting electrons), supplemented by simple numerical calculations.

The thesis also contains a brief introduction to Kondo effect and the theory of Numerical Renormalization Group.

Keywords: Topological superconductors, Majorana fermions, Kondo effect, Non-Fermi liquids, Topological quantum computation, spin-orbit coupling, charging energy.

Acknowledgement

I like to express my immense gratitude to my thesis supervisor Henrik Johannesson for the precious support and encouragement during the project. Without his patient guidance and positive attitude in aiding me towards the completion of the Master thesis, I would have not tunneled through many barriers.

I wish to thank my examiner and program coordinator Thilo Bauch for supporting me throughout the thesis and my time at Chalmers. I extend my sincere gratitude to Erik Eriksson for his helpful assistance.

I would like to thank the Autumn School on Correlated Electrons 2015 for providing me an opportunity to have many interesting discussions and also serving as a motivation to complete my thesis. Last but not least, I thank all my friends and family.

Contents

Chapter 1

Introduction

This thesis revolves around the quantum wire realization of the topological Kondo effect [1], primarily the analysis of it, focusing on the role of charging energy and exploring possible improvements. Chapter 2 begins with an introduction to Fermi liquids and their deviating behavior, citing the necessity to look beyond Landau's realms, which leads to the origin of Non-Fermi liquids. It is the desire to grasp the physics of Non-Fermi liquids that serves as an underlying motivation for the project.

This is followed, in chapter 3, by a brief overview of the Kondo effect. Herein a short rundown of the numerical renormalization group is given to aid the understanding of the multichannel Kondo effect, and how to locate the fixed point which exhibits Non-Fermi liquid behaviour. The multichannel Kondo model is then dealt with in detail, in particular, describing the critical overscreening of the impurity spin and the exotic physics associated with it. The chapter finally outlines the possibility of realizing Kondo effect in quantum dots and semiconducting heterostructures.

Chapter 4 is subsequently dedicated to the topological classification of systems into topological insulators and topological superconductors. It exposes the characteristics of the elusive Majorana fermions appearing in condensed matter systems and their potential applications in quantum computing. The rest of the chapter is devoted to the realization of a 1D spinless p-wave superconductor that hosts Majorana fermion bound states at its ends.

Finally, chapter 5 elucidates the set-up consisting of two topological superconducting wires to realize topological Kondo effect and the role of charging energy of the superconducting island that governs the energy spectrum. The significance of parity in electron transport across the superconductor is discussed, ultimately delving into the emergence of the Kondo problem in the effective model.

Chapter 2

Physics beyond Landau's paradigms

For more than half a century, our understanding of the metallic state has relied primarily on Landau's Fermi-liquid theory [2]. While the Fermi gas paints a picture of non-interacting fermions, the Fermi liquid provides an effective description of interacting fermions. Accordingly the metallic state is accounted for; on the other hand, the numerous different states of matter are distinguished by identifying the broken symmetry. This idea of spontaneously broken symmetry expressed by an order parameter forms the basis for Ginzburg-Landau theory of phase transitions [3]. Though Fermi liquid theory presents an astonishingly successful description of many metals, it has become increasingly evident that the behaviour of many complex materials, such as the most notorious problem of high temperature superconductors and certain f-electron materials fall outside this Fermi liquid picture [4]. As it turns out, the order parameter too fails to capture the true nature of the state of these materials violating the Ginzburg-Landau paradigm [5]. As experiments continue to unveil novel materials with unexpected metallic behaviour, theoretical advances have questioned the inadequacies of these paradigms in the general understanding of correlated matter. Thus it becomes pertinent to explore the physics beyond Landau's paradigms.

2.1 Fermi Liquids and Non-Fermi liquids

2.1.1 Fermi Liquids

The key ideas of Landau's Fermi liquid theory, fundamental to the understanding of Quantum many-particle systems, are the notion of adiabatic continuity and quasiparticle. For a non-interacting Fermi system at zero temperature, the ground state consists of a filled Fermi sea of electrons occupying all states below the Fermi energy $\boldsymbol{\epsilon_F}$ and the Fermi momentum $\boldsymbol{p_F}$. The distribution function can be easily described by a step function of the form

$$n(p) = \theta(p - p_F) = \begin{cases} 1 & \text{when } p < p_F \\ 0 & \text{when } p > p_F. \end{cases} \tag{2.1}$$

The concept of adiabatic continuity generalized by Anderson [6] involves the idea that, often the strongly interacting system retains some of the properties of its non-interacting parent. With the interactions being slowly turned on in a non-interacting system, there is a continuous mapping of the low energy eigenstates of an interacting system with that of the reference non-interacting Fermi sea. Thus the quantum numbers associated with the excitations of non-interacting electrons are still valid even after the interactions are fully applied, provided no phase transition occurs. However, the electrons in the interacting system are not free electrons anymore but electron-like 'quasiparticles'. This is because wavefunctions and energies associated with the interacting system are different from that of their non-interacting counterpart. The total energy of the interacting system is not merely the sum of single-particle energies as observed in a free Fermi gas. There is a difference in energy which is accounted for by a change in effective mass of the particles. This energy of the quasiparticles also depends on the quasiparticle distribution which no longer follows that of the non-interacting Fermi system described above (2.1). However, a discontinuity is still observed as shown in Figure 1.1 below.
The discontinuity in the electron distribution function at the Fermi level is given by quasiparticle weight Z. In a non-interacting system, the eigenstates are the single-electron states, hence the spectral function of free electrons is a delta function with $Z = 1$, same as the probability of finding an electron in an occupied state below the Fermi level. In the interacting system however, the eigenstates represent the quasiparticles, making $Z < 1$ since the probability of finding an electron in a given state while it is interacting with other electrons is less than 1. Just like particle-hole excitations of the non-interacting system, a quasiparticle with momentum $\boldsymbol{p}$ close to $\boldsymbol{p_F}$ can undergo scattering

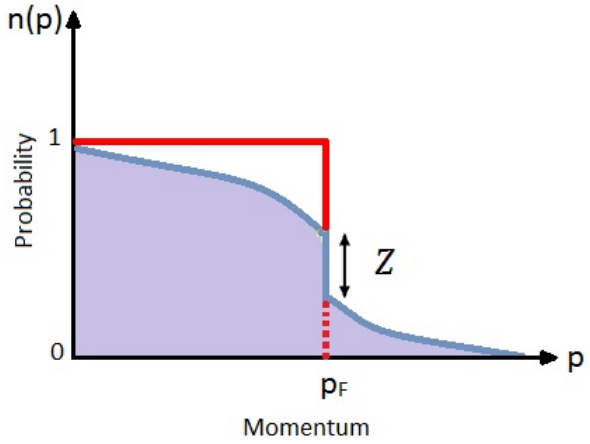

Figure 2.1: Probability distribution of the non-interacting system (red line) and the interacting Fermi liquid (shaded region) with the discontinuity Z.

into another state $\boldsymbol{p'}$, creating quasiparticle-quasihole excitations. This leads to a decay rate of $\sim |\boldsymbol{p} - \boldsymbol{p_F}|^2$, reflecting a finite lifetime thus causing the quasiparticles to be well-defined and stable close to the Fermi level. This also illustrates the $\boldsymbol{T^2}$ low-temperature resistivity of the metal due to electron-electron interactions. In the same way, the quasiparticle does recover the free electron expressions for specific heat and magnetic susceptibility as the temperature goes to zero, thus confirming the success of Fermi liquid theory.

2.1.2 Non-Fermi liquids

Materials which do not display Fermi liquid behaviour are called non-Fermi liquids [7]. Some of the examples of such materials with properties appearing to be inconsistent with Fermi liquid theory that have been experimentally discovered include,

- High-temperature superconductors - The unusual metallic behaviour of cuprates and the effective two-dimensional nature of CuO_2 planes and its properties can not be accounted for by the Fermi liquid theory [8][9].
- Many metallic alloys containing elements such as Ce or U with partially filled f-shells or, Fe or Ru with partially filled d-shells - The properties in bulk d- and f-electron metals were found to violate the Fermi liquid behaviour at low temperatures [10][11].

- Edge states of quantized Hall systems - the appearance of fractionally charged objects in the fractional quantum Hall effect. Contrary to the Fermi liquid, switching off interactions in a fractional quantum Hall system does not produce a unique non-interacting reference state but a number of degenerate ground states [12].

Theoretically the concept of Landau's Fermi liquid has been found to break down in the following cases,

- In one-dimension. In one-dimensional metals, the electrons are unstable and decay with a rate $\sim T$ [7][13], into two separate quasiparticles, spinons and holons carrying the electron's spin and charge respectively. The concept which replaces the Fermi liquid theory in one dimension is called the Luttinger liquid [14].

- Near quantum critical points. When a phase transition occurs at absolute zero, the quantum fluctuations cause the quasiparticles to scatter drastically and become unstable, ceasing their Fermi liquid behaviour [15].

- In non-trivial impurity models. In a Kondo model, a magnetic impurity scatters electrons near the Fermi level. While the ordinary single-channel Kondo model behaves as a Fermi liquid, the two-channel extension doesn't so. In general, Kondo models with multiple electron channels or interacting impurities follow the physics of non-Fermi liquids [16].

Approaches towards explaining these phenomena and developing new ideas and concepts have lead to the development of numerous mathematical methods and experimental techniques. Thus the understanding of non-Fermi liquids has become an important challenge in condensed matter physics with the breakdown of Landaus paradigms in correlated quantum phases.

2.2 Phase transitions and order parameters

As mentioned at the start, in the Ginzburg-Landau paradigm of phase transitions, an order parameter is defined to classify and distinguish the different states of matter. Because one of the symmetries of the system is broken spontaneously as the system moves from a disordered to an ordered state, the order parameter is defined as the measure of the degree of order across the phase boundaries [3]. In fact, the order parameter is zero on the high-temperature, disordered side and non-zero in the ordered, low-temperature

side of the phase transition. A common example of a phase transition is a disordered liquid crystallizing to form a solid crystal of long range order which breaks the continuous translational symmetry, as each point in a crystal does not have the same properties as observed in a fluid. Similarly in a ferromagnetic phase, the magnetic moments undergo a spontaneous transition from a disordered phase with no net magnetization to an ordered phase with a non-zero net magnetization where the magnetic moments are aligned in a definite direction, resulting in a degenerate ground state. As the spins (angular momenta) change sign during time reversal, the spontaneous magnetization in a ferromagnet breaks the time-reversal symmetry. While the order parameter in a one-dimensional crystal is the local displacement, the order parameter in a ferromagnetic material is the local magnetization. Likewise the low-frequency elementary excitations are sound waves or the phonons in crystals, and in the latter, the massless excitations are the spin waves called the magnons.

In the same way, the superconducting phase transition of conventional superconductors can also be explained in terms of symmetry breaking [17]. Herein the electrons experience an attractive force due to phonon mediated interactions and become bound to each other and condensate to form Cooper pairs. The many single-electron wave functions now transfigure into a collective wave function representing the condensate, breaking the global phase U(1) symmetry, with the pair density acting as the order parameter.

2.3 Breakdown of Landau's paradigms

The prominent instance where the Fermi liquid theory breaks down is at a quantum critical point. At second order phase transitions, the fluctuations corresponding to the order-order correlations occur over longer wavelengths causing dramatic scattering of the quasiparticles [5]. With the lifetimes of the approximate eigenstates now much reduced, the quasiparticles wither away even before the interactions are turned on adiabatically. Secondly, the well-known example as mentioned previously that violates Ginzburg-Landau symmetry breaking paradigm is the fractional quantum Hall effect, as the many phases in these systems exhibit the same symmetry. Moreover, these correlated phases display a new kind of 'order' which simply cannot be encapsulated by a Ginzburg-Landau order parameter. Such order which defies the old notion of spontaneous symmetry breaking theory is called *topological order* [18]. While the degenerate ground states previously mentioned were a reflection of the spontaneous symmetry breaking during a quantum phase transition, here the degenerate ground states that arise reflect the topologi-

cal order of the system. Such degeneracy which depends on the topology of the geometry of the system is called *topological degeneracy* and it is robust against perturbations [19]. As opposed to Landau's concepts wherein the quantum numbers are retained and the symmetry is broken, the FQH states possess different quantum numbers of topological origin known as *topological quantum numbers* [18] whilst the symmetry is preserved. Here the topological deformations define the adiabatic continuity. The continuous phase transition between these different phases in the fractional quantum Hall effect cannot be explained by fluctuations in an order parameter alone since there is no order parameter to begin with. The ideas of Landau not only break down at the correlated phases but also at the zero temperature quantum phase transitions.

2.4 Exploring beyond Landau's paradigms

Thus in effect, be it the topologically ordered phases or the multichannel Kondo effect or the heavy fermion metals, to understand any non-Fermi liquid behaviour, exploring the physics beyond Landau's paradigm becomes vital. Of the above, the non-trivial Kondo models are appealing in particular because they likely pave the way for understanding the formation of heavy fermions [16]. Moreover, the simplest one-channel Kondo model also exhibits the interesting phenomenon of asymptotic freedom providing for a simple variant of the very mechanism behind quark confinement in QCD [20]. In the case of the two-channel Kondo model, the anti-ferromagnetic Kondo interaction causes a cooperative enhancement of the interactions between the impurity spin and the conduction electrons resulting in an extraordinarily strong effective Kondo coupling, which because of the competition between the two screening channels makes the resulting ground state unstable. In a quantum dot, a Kondo mediated transport results in enhanced conductance. However, realizing the two-channel Kondo effect experimentally in a quantum dot does become tricky with the requirement of fine tuning of the applied bias and other parameters [21]. External parameters such as temperature and magnetic field, and various processes such as thermal fluctuations and microwave radiations in the quantum dot may also cause decoherence of the Kondo singlet state destroying the Kondo effect.

Recent developments have lead to the possibility of realizing localized Majorana Fermions at the ends of topological superconductors [22][23]. The degeneracy of the ground state associated with these Majorana modes is topological in nature which is robust under perturbations and gives rise to nonlocal zero-energy degrees of freedom. Moreover, the quantum spins as-

sociated with these nonlocal modes in turn give rise to a novel Kondo effect topologically protected against perturbations, resulting in a highly robust non-Fermi liquid behaviour, the "topological Kondo effect" [1]. As topological qubits can be encoded in these nonlocal zero-energy modes, they form the basis for fault tolerant quantum computation [24].

Therefore, study of this robust non-Fermi liquid, the topological Kondo effect can lead to better understanding of the mesoscopic transport in the superconducting structures that support Majorana fermions. This may pave way for the realization of fault tolerant computation using Majorana fermions.

Chapter 3

Kondo effect

The Kondo effect arises as a magnetic impurity scatters conduction electrons near the Fermi level with a spin-exchange interaction causing an increase in resistivity of the metal at low temperatures. It was first observed during the 1930s that metals such as gold and copper exhibit a finite resistance at low temperatures [25]. Later studies of gold and copper with iron impurities revealed that the presence of magnetic impurities dramatically changes low-temperature resistivity in metals [26]. The phenomenon as initially explained by Jun Kondo in 1964 is simply due to the interaction of spins [27]. The local magnetic moment of the impurity aligns parallel or anti-parallel to the spin of nearby electrons corresponding to a ferromagnetic or antiferromagnetic interaction and brings about a spin-exchange scattering of electrons. Jun Kondo showed that the resistivity ρ due to spin exchange scattering increases logarithmically with decrease in temperature $\rho \sim -\ln(T/T_K)$. However, the theory put forward by Kondo remains valid only till a particular temperature called "Kondo temperature", T_K and cannot be trusted for temperatures far below. At T far below T_K, the spin-exchange interaction between the impurity and electrons rapidly grows with decrease in temperature eventually leading to a coupling of a single electron with the impurity to form a singlet. Understanding of the physics below Kondo temperature is facilitated by the theory of *Poor Man's Scaling* [28] developed by Anderson and the concept of *Numerical Renormalization Group* invented by Wilson [29].

The Kondo effect therefore has two regimes, a strong coupling and a weak coupling regime very analogous to asymptotic freedom behind quark confinement in QCD. In the *weak coupling* regime ($T > T_K$) the magnetic impurity scatters electrons which increases logarithmically with decrease in temperature analogous to the free quarks weakly interacting at high energies and with *strong coupling*($T < T_K$), magnetic moment of the impurity is screened by single electrons which are bound to it forming a singlet state much alike

the quarks interacting strongly at low energies where they bind to each other. The Kondo model of a single impurity is given by the Hamiltonian,

$$H = \sum_{k,\sigma} \epsilon_k c^\dagger_{k\sigma} c_{k\sigma} + J \sum_{k,k',\sigma,\sigma'} c^\dagger_{k\sigma} \boldsymbol{\sigma}_{\sigma\sigma'} c_{k'\sigma'} \cdot \boldsymbol{S} \tag{3.1}$$

where the first and second term represent the kinetic energy and electron-impurity spin-exchange interaction of a sea of spin-1/2 conduction electrons respectively. S represents a spin-1/2 magnetic impurity and J the exchange coupling between the impurity and conduction electrons. A negative J corresponds to a ferromagnetic interaction and a positive J implies an antiferromagnetic interaction.

While the single-impurity Kondo model is well-understood, a Kondo model in general can be associated with multiple scattering channels and/or several coupled impurities. Also the ferromagnetic Kondo model remains essentially trivial as the spin of the impurity is not screened by conduction electrons, in the strong coupling low-temperature regime, the impurity fundamentally remains free and is decoupled from the conduction sea. However, such is not the case with respect to antiferromagnetic coupling as the impurity is screened by conduction electrons which strongly couple to form a singlet under low energies. A simple perturbative approach cannot explain such low-temperature phenomena of the Kondo model and calls for non-perturbative treatments such as numerical renormalization group to understand the physics below Kondo temperature.

3.1 Concept of Renormalization

In condensed matter systems, the energy scales at which various physical processes take place may vary. In the Kondo effect, the kinetic energy of the free conduction electrons is typically of the order of several electron-volts while the energy scale of the electron-impurity interaction is only few meV. Therefore, to understand the physics in the low-temperature regime $T < T_K$, the Kondo model devised at higher energies needs to be scaled down to lower energies. This can be done by lowering an energy cutoff scale Λ [30]. An ultraviolet cutoff gives the maximal allowed energy of the excitations that are taken into account in the model, ignoring physical quantities and excitations with energies above the cutoff. Since only the low-energy (infrared limit) properties of the system are of primary interest, by successfully lowering the cutoff one focuses on the behaviour of the system at lower energies, thus eliminating any higher energy contributions. The system once renormalized is rescaled again to a new energy cutoff, and integrating out the degrees

of freedom outside the newly rescaled energy range results in an effective coarse-grained Hamiltonian after rescaling of the cutoff energy.

Thus, it is the cutoff dependence of physical quantities that is the premise of renormalization group. The procedure of renormalization group transformation can be summarized into following steps,

1. Discretizing the energy scale with cutoff energy (Λ).

2. Integrating out states at energies above the rescaled cutoff and renormalizing the coupling constants ($J \to J(\Lambda)$) to low energies.

3. Rescaling the cutoff energy ($\Lambda \to \Lambda'$) resulting in a new Hamiltonian.

Repeating the above steps, the RG transformation leads to a *fixed point* Hamiltonian that is no longer sensitive to iteration, having filtered out fine details of the original high-energy model and retaining only observables that remain universal. The RG transformation of a high energy model Hamiltonian continuously evolves with Λ and flows towards these fixed points which are scaling invariant and hence belong to the same universality class. Therefore, with a running energy scale Λ and cutoff dependent coupling constant, the RG transformation causes a renormalized flow of the coupling constant towards the fixed point resulting in a running coupling constant $J(\Lambda)$ [30].

For the simple one-channel Kondo model there exists two fixed points as cutoff energy scales with temperature.

- At $\mathbf{T = \infty}$, in high energy scales where $\Lambda \to \infty$, the coupling constant is $J \to 0$ denotes weak coupling regime.

- At $\mathbf{T = 0}$ low-temperature regime, low energy physics dominates as coupling constant flows to infinity $J \to \infty$.

In a ferromagnetic Kondo model the coupling at lower energies is negligible and hence $J \to \infty$ fixed point is unstable and only the weak coupling fixed point at $J = 0$ is stable. But in an antiferromagnetic Kondo model, the $J = 0$ weak coupling point is unstable and $J(\Lambda) \to \infty$ gives the strong coupling fixed point describing the stable singlet state validating the low-energy theory of the Kondo model below T_K. Thus these two fixed points for antiferromagnetic coupling, $J = 0$ (unstable when renormalizing to low energies) and $J = \infty$ (stable at low energies) are indeed hallmarks of an asymptotically free theory.

3.2 Multichannel Kondo problem

Whereas the single-channel Kondo model by far renormalizes to a Fermi liquid at low temperatures, the so-called multichannel Kondo problem exhibits unusual non-Fermi liquid behaviour. Nozires and Blandin [31] formulated the multichannel Kondo model for an impurity of arbitrary spin S with M orbital channels as

$$\begin{aligned} H &= \sum_{k,\sigma,\mu} \epsilon_k c^\dagger_{k\sigma\mu} c_{k\sigma\mu} + J \sum_{\mu=1}^{M} \boldsymbol{S} \cdot \boldsymbol{\sigma}_\mu \\ &\text{with } \boldsymbol{\sigma}_\mu = \sum_{k,k'\alpha,\beta} c^\dagger_{k\alpha\mu} \boldsymbol{\sigma}_{\alpha\beta} c_{k'\beta\mu}. \end{aligned} \tag{3.2}$$

Here $\boldsymbol{\sigma}$ denotes the vector of Pauli matrices representing the spin of the conduction electrons in the channel with index μ ($\mu = 1, 2, ..., M$) and J denotes the exchange coupling which is taken to be antiferromagnetic. The ferromagnetic case is for now ignored as the coupling stays weak at lower energies.

Three different cases are observed in a multichannel Kondo model with antiferromagnetic interaction depending on the number of channels M and spin S of the impurity [31].

- $M < 2S$: when the number of channels is less than the magnitude of the impurity spin S, the impurity is not effectively screened and has a net spin that is not compensated resulting in a *underscreened Kondo model*.
- $M = 2S$: *Perfectly screened Kondo model* where the impurity spin is completely screened and compensated for, with the number of scattering channels being equal to the impurity spin size. This is much alike the single-channel Kondo model.
- $M > 2S$: the case of *overscreening* occurs when the number of channels is larger than the magnitude of the impurity spin, resulting in an unstable ground state which is a non-Fermi liquid.

The resulting singlet ground state in the first two cases (with a residual decoupled spin in the underscreened case) is a Fermi liquid state and does not display any unusual behaviour [32]. While both the underscreened and overscreened multichannel Kondo models have net spin, the differences between the two and the intriguing physics of an overscreened multichannel Kondo model can be easily explained in a renormalization group language [30].

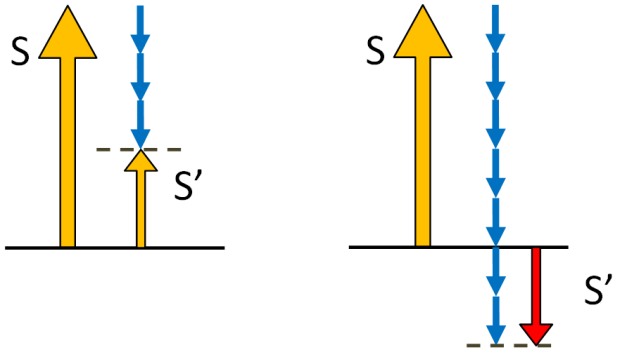

Figure 3.1: Multichannel Kondo effect (a) Underscreened case $M < 2S$ (b) Overscreened case $M > 2S$

Underscreening

In an underscreened model, $M < 2S$, once the cutoff energy Λ goes below the Kondo temperature, the impurity is partly screened by antiferromagnetic coupling to the conduction electrons. The uncompensated net spin given by $S' = S - M/2$ has same spin direction as S as shown in Figure 3.1(a) and can still interact with electrons. However as all orbital channels are already occupied by electrons of opposite spin leaving no room for further antiferromagnetic interaction, the residual coupling of the resultant spin J' is therefore ferromagnetic. The orbital channels of the conduction electrons can be envisioned as spherical shells surrounding the impurity, with each shell of electrons carrying opposite spins (depicted in Figure 3.2) because of the Pauli principle. Hence, only the next channel of electrons with spin parallel to S' can interact with the residual spin S'. Since ferromagnetic coupling scales to weak coupling, $J' = 0$, the RG flow of the antiferromagnetic coupling is towards $J(\Lambda) = \infty$ fixed point, which is now stable.

Overscreening

In an overscreened case, as $\Lambda \to 0$ the conduction channels try to screen the impurity spin to form a Kondo singlet in the strong coupling limit $J(\Lambda) \to \infty$. However, since there is now a surplus of channels, the screening will overcompensate the spin-up impurity, resulting in a net spin $S' = M/2 - S$ pointing down as seen in Figure 3.1(b). Much alike the underscreened case, there is no extent for spin down electrons to interact with the impurity as they have occupied all available states and only spin-up electrons of the next

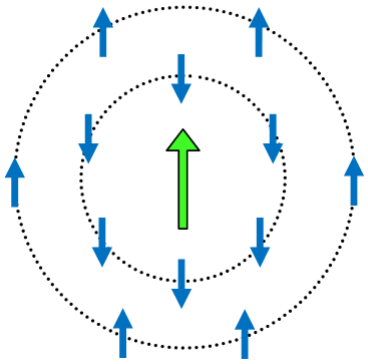

Figure 3.2: Electron orbital channels as 3D shells surrounding and screening the impurity in a multichannel Kondo problem.

set of orbital channels interact with the impurity. The difference lies in the detail that S' in the underscreened case has the same spin as the impurity S, but in the present case the effective spin S' is opposite in direction to S making the residual coupling J' to be anitferromagnetic. Nevertheless, when the antiferromagnetic coupling J' flows towards the strong coupling fixed point $J'(\Lambda) \to \infty$, it will explode yet again like J did. One thus expects that the strong coupling fixed point, $J(\Lambda) = \infty$, is unstable and RG flows to a finite but stable intermediate coupling fixed point as illustrated schematically in Figure 3.3. This conclusion is corroborated by a formal RG calculation.

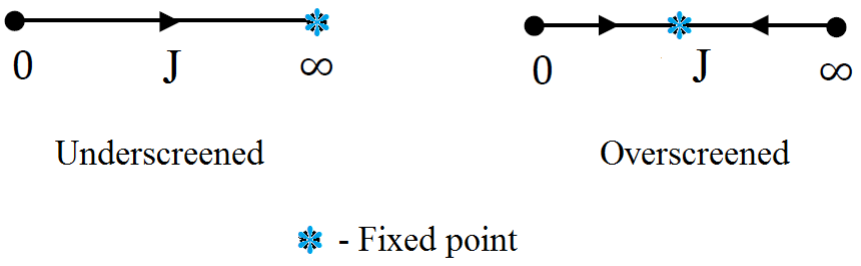

Figure 3.3: Renormalization group flows of the running coupling $J(\Lambda)$ [30].

The ground state characterized by this intermediate coupling fixed point exhibits non-Fermi liquid behaviour. Using Bethe ansatz or conformal field techniques, an exact solution to the multichannel Kondo problem can be

obtained and the intermediate coupling fixed point can be identified [33][34]. The simplest example of a multichannel Kondo problem is the case of the overscreened spin-1/2 two-channel Kondo model. The two-channel Kondo problem is of particular interest as it paves way towards observing non-Fermi liquid behaviour, has practical applications as a two-level system, and also gives a better insight into the physics of an intermediate-coupling fixed point.

3.2.1 Two-channel Kondo model

In a two-channel Kondo effect, a spin-1/2 impurity is surrounded by two scattering channels $M = 2$. The sea of conduction electrons in these two channels do not interact with each other and are perceived only by the impurity. In the weak-coupling high-temperature regime, conduction electrons in both channels are scattered by the spin-1/2 impurity. However, the physics in the low-temperature strong coupling limit becomes particularly interesting depending on the coupling of the two channels with the impurity. If a and b are the two conduction channels, then from (3.2) the two-channel Kondo Hamiltonian takes the form,

$$H = \sum_{k,\sigma,\mu=a,b} \epsilon_k c^\dagger_{k\sigma\mu} c_{k\sigma\mu} + J_a \boldsymbol{S} \cdot \boldsymbol{\sigma}_a + J_b \boldsymbol{S} \cdot \boldsymbol{\sigma}_b. \tag{3.3}$$

Even for a small channel asymmetry, $J_a \neq J_b$, the stronger coupled channel screens the impurity and thus the two-channel Kondo model behaves just like an ordinary single-channel model. In other words, channel asymmetry causes the channel that is coupled stronger to flow towards the strong coupling limit $J \to \infty$, and the weakly coupled channel flows to the weak coupling fixed point $J = 0$. However, when both channels have equal coupling strength, $J_a = J_b$, then exotic overscreened behaviour ensues, resulting in an unstable ground state [32].

Because of the symmetry of the two channels in this case, the impurity cannot favour a single channel to form a singlet. Therefore the resultant state has a net spin $S' = M/2 - S = -1/2$ as the two spins bind to the impurity. This state with a net spin $-1/2$ behaves as a new spin-1/2 impurity, and having two channels to interact with, undergoes another Kondo effect which in turn results in a new state with spin $+1/2$ and so on. This behaviour is illustrated in Figure 3.4. Therefore, the ground state in the strong coupling limit is unstable and flows towards a finite intermediate coupling fixed point, which is only stable at the critical point $J_a = J_b$. As a result, the impurity is never completely screened.

The Bethe ansatz solution of the two-channel Kondo problem gives the ground state associated with the intermediate coupling fixed point and it has

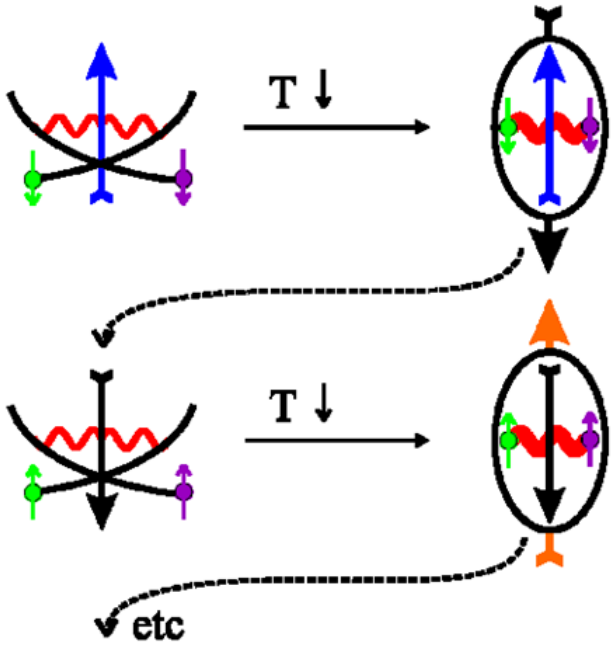

Figure 3.4: Two-channel Kondo effect where the impurity spin $+1/2$ interacts with two conduction channels and forms an effective residual spin which has a net spin $-1/2$. The residual spin acts as a new spin-1/2 impurity and interacts with two conduction channels going through another Kondo effect and so on [7].

a residual entropy of $1/2 \ln 2$ [33]. This residual entropy can be interpreted by following an Abelian bosonization approach which identifies this fractional entropy as a Majorana fermion mode [35]. Majorana fermions are fermions that are their own anti-particles and the appearance of Majorana fermions as quasiparticles in condensed matter systems is discussed in detail in forthcoming chapters. The Abelian bosonization of the two-channel Kondo model results in a resonant-level Kondo model and is analogous to the Toulouse limit of the single-channel Kondo model [36]. Thus, a reformulation of the two-channel Kondo problem in terms of Majorana representation helps to understand the low-energy fixed point. Another method involves compactifying the two-channel Kondo model by expressing the Hamiltonian in terms of three Majorana fermion modes that describe the decoupled spin degrees of freedom. This is achieved by separating spin and charge into independent degrees of freedom and focusing exclusively on the former [37]. In fact, a channel signifies the internal degrees of freedom of conduction electrons coupled to the impurity. Since a Majorana fermion is only half a fermion, it can

be perceived that only half the impurity degrees of freedom are coupled to the conduction electrons, therefore leading to a suitable interpretation of the residual entropy $1/2 \ln 2$. Besides it has been shown that a Majorana formulation of the two-channel Kondo model emerges naturally as a representation of the algebra associated with total spin currents of the two channels [38]. It is achieved by following a conformal field theory approach [39][34]; when the interaction term of the two-channel Kondo model is defined in terms of spin currents of the conduction electrons and impurity spin, the spin current operators satisfy Kac-Moody algebra commutation relations of non-Abelian symmetry groups pertaining to the number of channels. As a result, the spin currents of the two-channel Kondo model is found to obey an $SU(2)$ level-2 algebra. And by representing these spin currents by way of three Majorana fermion operators that reproduce aforesaid $SU(2)$ level-2 algebra, an equivalent Majorana fermion representation of the two-channel Kondo model is readily obtained [38]. As a result, by conveniently expressing the two-channel Kondo model in a Majorana representation, the physics of low-energy fixed point can be analysed effectively.

Similarly it has been shown that a four-channel spin-1/2 Kondo model can be mapped to an equivalent two-channel spin-1/2 model but with spin-1 conduction electrons [40]. A subsequent Abelian bosonization of the two-channel Kondo model with spin-1 conduction electrons greatly facilitates the determination of low-temperature properties.

These multichannel Kondo effects can be used to explain some aspects of the physics of heavy fermion systems. In fact, the simplest case of a two-channel Kondo model is well suited to explain the properties of many heavy fermion alloys and compounds [16]. While many actinide and rare-earth impurities exhibit exotic Kondo effects, the multichannel Kondo model discussed so far fits URu_2Si_2, UPd_2Si_2, UPd_2Al_3 and $UBe_{13}Pt_3$, all of which are heavy fermion superconductors. And $Y_{1-x}U_xPd_3$ exhibits residual entropy and thermodynamics similar to that of a two-channel Kondo problem. Further experimental data on the two-channel Kondo model as well as detailed accounts of solvable methods for the multichannel Kondo problem can be found in [41].

3.3 Kondo effect in Quantum dots

A quantum dot is nothing but a solid state device, a semiconductor box capable of holding a well-defined number of electrons. Electron transport through the quantum dot is possible when it is connected to two leads. A weak coupling between the source, drain leads and the dot results in a tun-

nel barrier and when the coupling energy is small compared to the charging energy, electrons are confined to the dot ensuing in a well-defined particle number N. The quantization of electronic charge e due to the charging energy requires more than a single-particle description to describe the dynamic electron-electron interactions. The electron transport phenomena arising out of such a single-electron box with dynamic charge fluctuations is called *Coulomb blockade effect* [42]. It is now evident that in a Coulomb blockade regime, first order tunneling is scarce and is suppressed owing to the presence of two tunnel barriers. However, second order co-tunneling processes are possible such that the electrons can tunnel readily through virtual intermediate states. A spin exchange tunneling enhances the electron transport between leads, increasing the conductance through the quantum dot [43], the very spin exchange scattering that causes an increase in resistivity in metals. Kondo effect in metals increases the resistance while the Kondo effect in quantum dots enhances the conductance, displaying the opposite behaviour [21]. This is due to constructive quantum interference effects between empty and doubly occupied virtual states on the dot and happens only when the dot is connected to leads by two separate tunnelling junctions. A quantum dot side-coupled to a lead has the same effect as a spin impurity in a bulk metal, causing increased resistivity. It should be noted that a Kondo effect arises in a quantum dot only when the number of electrons is odd, with the unpaired electron in the dot behaving as a localized spin-1/2 impurity. The electron tunneling through the dot experiences a spin flip. There is no enhanced conductance when electron occupancy is even, as it does not give rise to a Kondo effect.

There are several advantages in investigating Kondo physics of quantum dots. The Kondo effect can be simply switched on and off as a function of electron occupancy, i.e. odd and even occupancy. The characteristic Kondo temperature can be tuned in such devices and the behaviour of a localized impurity can be well observed [44]. The ability to design and control the parameters of semiconductor quantum dots facilitates study and experimentation of new Kondo regimes. In effect, observation of the exotic two-channel Kondo effect is deemed possible by carefully engineering semiconductor nanostructures and fine tuning the system [45][46][47][48]. Yet the very same fine tuning of parameters causes the non-Fermi liquid fixed point to be fragile and susceptible to perturbations. Therefore, to examine the exotic non-Fermi liquid behaviour of a two-channel Kondo model, a more robust system is desirable.

Chapter 4

Topological Insulators and Superconductors

A doughnut and a coffee mug are not any different to a topologist. Topology in the mathematical context deals with the study of properties of objects which are invariant under certain smooth and continuous transformations. These transformations, such as a doughnut being continuously deformed and reshaped in to a coffee mug with a handle on its surface, conserving its geometrical property as a torus, are called homeomorphisms. The property or quantity that is preserved under such homeomorphisms is known as topological invariant. If the topological invariants of two systems are different, then they are not topologically equivalent and do not exhibit any homeomorphism. The different classes of topological equivalence are defined based on a topological invariant, in the simple case just discussed, the 'genus' of the object. A genus is nothing but the classification of 2D surfaces based on the number of holes; the genus of a torus is one and the genus of a sphere is zero. The textbook by [49] Nakahara provides a good introduction to the subject of topology in physics.

Topology in the context of condensed matter physics comes in two varieties: symmetry-protected topological phases vs topologically ordered phases. The latter is exemplified by the fractional quantum Hall effect which (like other topologically ordered phases) can be described by a topological field theory. A hallmark here is that the topological invariant is encoded in the ground state degeneracy, with long range quantum entanglement as a defining characteristic. In contrast, symmetry-protected topological phases (like topological insulators and superconductors) have ground states with short-range quantum entanglement. Most of these systems can be understood by employing the tools of topological band theory. Since the topological super-

conductors are of primary concern in this thesis, we shall provide first an introduction to topological band theory in the next section.

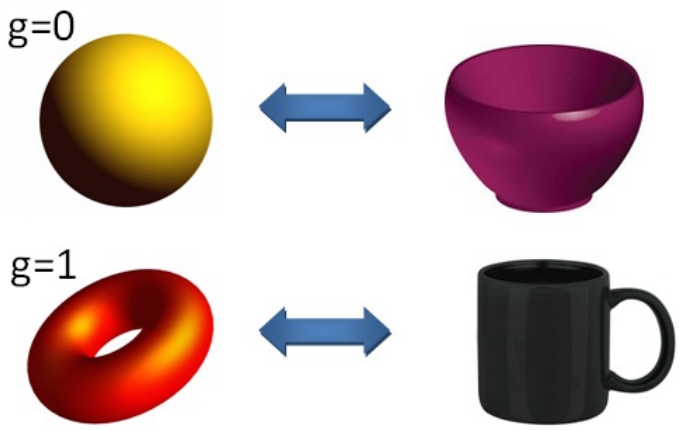

Figure 4.1: Examples of homeomorphisms of different topological classes defined by their genus. In the top (g=0) the sphere can be smoothly deformed into a bowl, at the bottom (g=1) a torus being smoothly changed into a coffee mug.

4.1 Topological Band Theory

An insulator and a semiconductor, much like the doughnut and a coffee mug, are said to be topologically equivalent. In both an insulator and semiconductor, the conduction band states are separated from the valence band states by an energy gap but it is the size of the energy gap that tells apart a semiconductor from an insulator. The crystal momentum in 2D is defined on a torus and not on an infinite plane as it is periodic in both directions. A band structure is a mapping of this crystal momentum to the Bloch Hamiltonian $H(k)$. The energy of the band structures is described by the eigenvalues $E_n(k)$ of this Hamiltonian. The concept of topology is employed in the band theory of solids such that the Hamiltonian describing an insulator can be smoothly deformed into the Hamiltonian of a semiconductor without closing the energy gap, making them topologically equivalent [50]. However, not all spectra with a finite energy gap are topologically equivalent, the integer quantum Hall state being a counterexample. The band structures thus fall into topological classes and the different classes of topological equivalence

are classified based on a topological invariant playing a role analogous to the genus in the example discussed above.

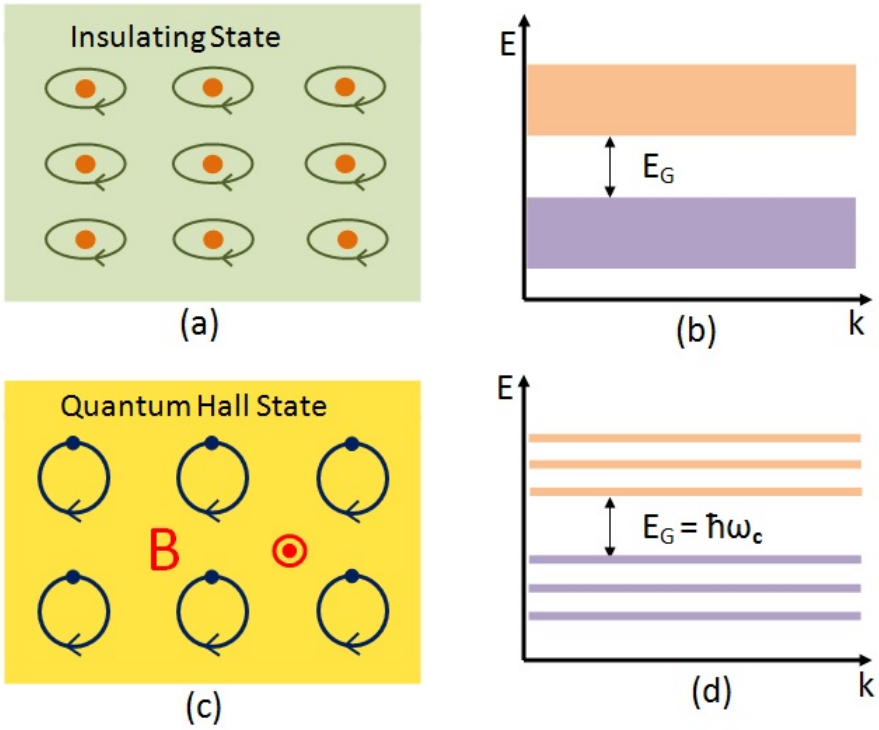

Figure 4.2: (a) An atomic insulator, (b) band structure of an insulator, (c) an integer quantum Hall state illustrating the electrons moving in cyclotron orbits, (d) shows the Landau levels with a band gap separating the occupied from the unoccupied Landau levels [50].

The integer quantum Hall effect is observed in two-dimensional electron systems placed in a strong magnetic field. The electrons then move in cyclotron orbits perpendicular to the magnetic field, leading to a massively degenerate spectrum of quantized Landau levels. The Landau levels are quantized with an energy $E_m = \hbar\omega_c(m + 1/2)$. Similar to the band structure, an energy gap separates the empty Landau levels from the occupied levels. Nevertheless, in an integer quantum Hall state, when an electric field is applied, the drift of cyclotron orbits causes a Hall current to flow, unlike an ordinary insulator. The quantised Hall conductivity of the Hall current is given by,

$$\sigma_{xy} = ne^2/h. \tag{4.1}$$

It is here the topological invariant n becomes relevant as it gains physical significance with the n in the Hall conductance [50]. With the n being a

topological invariant (a Chern number in the case of the integer quantum Hall effect), the Hall conductance remains accurate as n stands robust against any local perturbations ("continuous deformations of the Hamiltonian") that do not close the gap. It should also be noted that the presence of an external magnetic field here breaks the time reversal symmetry.

In summary, the concept of topology applied to gapped band structures has resulted in a topological classification of gapped band structures with a topological invariant distinguishing different states. In the paradigm example of the integer quantum Hall state, it differs from an ordinary insulator by being associated with a nonzero Chern number.

4.1.1 Edge states and bulk-boundary correspondence

One remarkable outcome of topological band theory is the existence of gapless edge states at the interface when two states of different topological classes, or a topologically non-trivial state with the vacuum, are put in contact together. When two quantum states of the same topological class are put together, the interface does not support gapless states. It can be seen that the change in topological invariant across the interface from one state to the other causes the closing of energy gap resulting in gapless conducting states.

In an interface between an integer quantum Hall state ($n = 1$) and an ordinary insulator ($n = 0$), the Chern number changes by $\Delta n = 1$. This change is possible only if the energy gap vanishes at the interface, resulting in low-energy electronic states bound to the interface. The interface between a quantum Hall state and an insulator gives rise to chiral edge states [50]. The dispersion of the edge states can be changed by modifying the Hamiltonian near the surface. A single edge state can be described by a single band crossing the Fermi energy once, connecting the valence band to the conduction band with a positive group velocity. If the Hamiltonian is varied smoothly such that the edge state crosses the Fermi energy three times, then additional modes arise to the left and the right with a positive group velocity twice and a negative group velocity once. The difference Δn between the number of right and left moving modes can never change and is preserved under these variations,

$$N_R - N_L = \Delta n. \tag{4.2}$$

As the variations are smooth, the perturbed (or deformed) Hamiltonian remains homeomorphic to the original one, conserving the Chern number of the bulk states. Here Δn is the difference in the Chern number across the boundary. This is known as the *bulk-boundary correspondence* [50].

4.2 Topological Insulators

Both the Hall conductivity and the Chern number as seen in (4.1) and (4.2) are odd under time-reversal and it is evident that the time-reversal symmetry is broken in non-trivial topological states. However there exists topologically non-trivial states that conserve time-reversal symmetry where spin-orbit interaction comes into play [50]. A topological insulator also known as a quantum spin Hall insulator with $n = 0$ is one such example. As we shall see, the non-trivial topological state here is associated with a nonzero value of a different kind of topological invariant, a so called Z_2 invariant.

Consider the time-reversal symmetry for spin-1/2 electrons represented by the antiunitary operator $\mathcal{T}^2 = -1$ which leads to a very important consequence, the *Kramers' theorem*. Kramers' theorem states that all eigenstates of a time-reversal invariant Hamiltonian commuting with $\mathcal{T}$ must be at least twofold degenerate [51]. If a non-degenerate state $|\xi\rangle$ were to exist such that $\mathcal{T}|\xi\rangle = c|\xi\rangle$ for some constant c, then it would mean that $\mathcal{T}^2|\xi\rangle = |c|^2|\xi\rangle$, which is not allowed as $|c|^2 \neq -1$, thus violating the time-reversal invariance. Because all angular momenta are reversed under $\mathcal{T}$ symmetry, if there is no spin degeneracy, the system will not be time-invariant. Kramers' degeneracy is simply the degeneracy between up and down spins in the absence of a magnetic field. Conversely, this degeneracy is lifted by the spin-orbit coupling. Importantly, the different classes of Hamiltonians preserving $\mathcal{T}$ symmetry that can be smoothly deformed without closing the energy gap can be distinguished topologically.

As a result some interesting non-trivial consequences are observed at the edge states (2D topological insulator) or surface states (3D topological insulator) of the sample [52]. Especially, the electronic states bound to the surface of the system at the points $k = 0$ and $k = \pm\pi/a$ of the Brillouin zone (where a is the lattice spacing) become interesting since these points turn out to be mirror images as they transform onto themselves under time-reversal. These states remain degenerate following Kramers' theorem in the absence of spin-orbit interaction. Now the degeneracy of different spins is lifted in the presence of spin-orbit coupling but Kramers' theorem requires for the states to remain degenerate. This is achieved through two possibilities resulting in two distinct topological configurations.

For one, when there is an even number of Kramers' pairs present, i.e. pairs of spin up and spin down states, these states can be pairwise connected at the Γ point, $k = 0$, leading to an opening up of a gap as shown in Figure 4.3 which shows band configurations of a fourfold degenerate edge state (two Kramers' pairs). With even number of Kramers' pairs, the edge states can be smoothly transformed from gapless to gapped configuration without violating

the Kramers' theorem and in fact, the edge states can be eliminated by pushing all the bound states out of the gap further into the bulk resulting in a trivial insulting state.

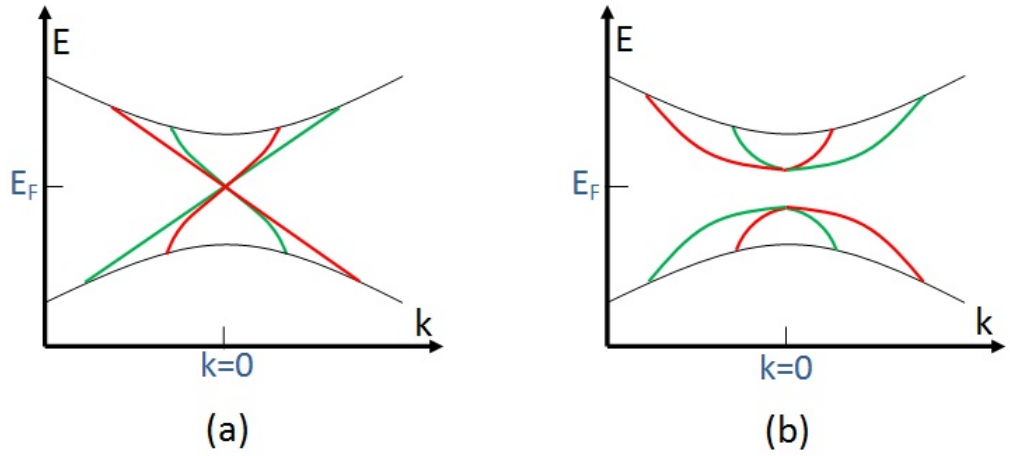

Figure 4.3: (a) A gapless configuration of edge states with two Kramers' pairs (b) A gapped configuration of the same under spin-orbit coupling. Opposite spins are indicated by red and green colours.

Now for the other, when the number of Kramers' pairs is odd, the state cannot be transformed into a gapped state without violating the Kramers' degeneracy. For example, when the system is doubly degenerate with one Kramers' pair as shown in Figure 4.4, opening up a gap would destroy the degeneracy and this is impossible in an a time-reversal invariant system. The edge states cannot be eliminated unlike the first case and the bands cross the Fermi level E_F odd number of times resulting in a topologically non-trivial state called the quantum spin Hall state with helical edges [50].

These two different topological configurations can be distinguished by a $\mathbb{Z}_2$ topological invariant ν, defined modulo 2 [50]. Thus, very much analogous to a Chern number, the topological invariant ν distinguishes a trivial insulator with $\nu = 0$ from a topological insulator with conducting edge states, $\nu = 1$, corresponding to even and odd number of Kramers' pairs respectively. The Chern number in these time-reversal invariant systems is zero. The bulk-boundary correspondence can be defined similarly based on the change in ν across the boundary,

$$N_K = \Delta\nu \mod 2. \tag{4.3}$$

Here N_K is the number of Kramers' pairs crossing the Fermi energy and

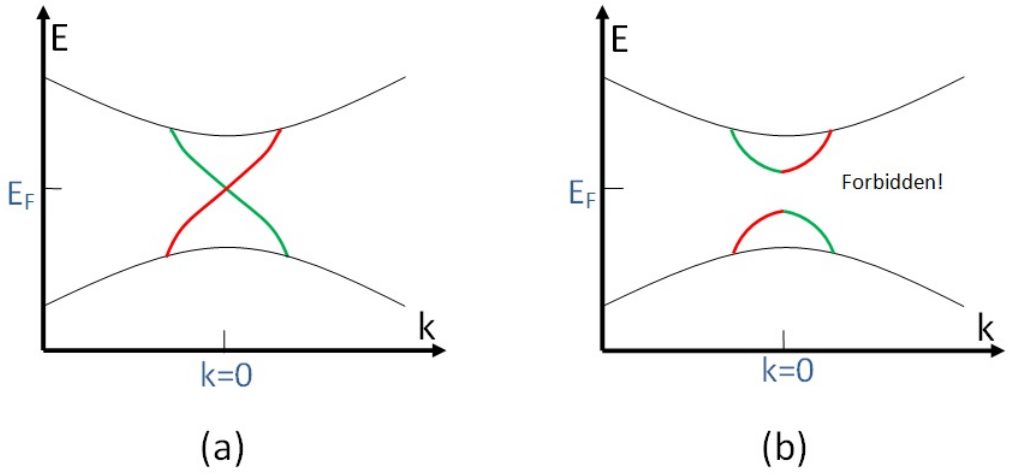

Figure 4.4: (a) A gapless configuration of edge states with one Kramers' pair (b) a forbidden gapped configuration showing the loss of degeneracy. Opposite spins are indicated by red and green colours.

$\Delta\nu$ is the change in topological invariant ν across the interface between two regions with topologically different states.

While the edge states appearing at the interface of an ordinary insulator and an integer quantum Hall state is due to change in Chern number, the edge states occurring at the surface between an ordinary insulator and a topological insulator is due to a change in the $\mathbb{Z}_2$ invariant making the edge states robust against smooth deformations and hence topologically protected. Figure 4.5 draws out a good comparison [53] between the two edge states. Ref.[54] gives a detailed mathematical formulation of the $\mathbb{Z}_2$ invariant ν.

4.3 Topological Superconductors

The topological band theory extended to superconducting states gave birth to the study of topological superconductors. Topological classification of superfluid states is also possible, the B phase of superfluid ^3He being an example [55]. In a superconductor, the condensate of Copper pairs is separated from the normal state by a superconducting energy gap. The Bogoliubov-de Gennes (BdG) Hamiltonian which gives the quasiparticle excitation spectrum of a superconductor consists of a superconducting gap similar to the band gap of an ordinary insulator. Since electrons are coupled in a superconductor, removing an electron from state 'k' uncouples the complementary electron in state '$-k$'. Thus creation of a quasihole at an eigenstate of energy $-E$ is same

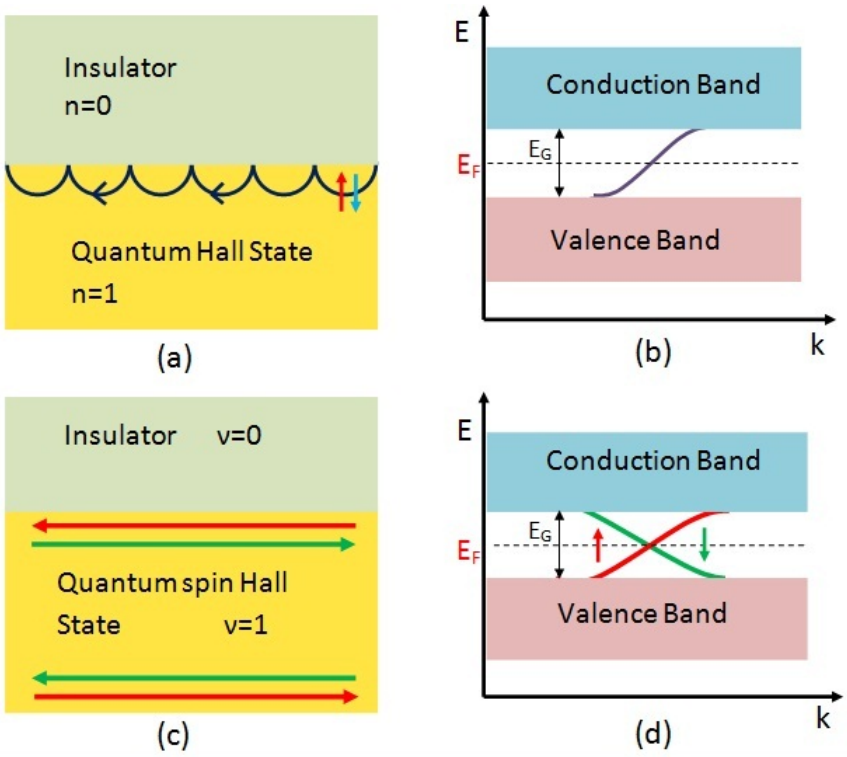

Figure 4.5: (a) Chiral edge states between an integer quantum Hall state and an ordinary insulator differentiated by the Chern invariant n and a band structure (b) describing the same. (c) Helical edge states between a quantum spin Hall state and an insulator distinguished by the $\mathbb{Z}_2$ invariant ν. (d) Band structure of the edge states with one Kramers' pair [52].

as removal of a quasiparticle at the eigenstate of energy E and a particle-hole symmetry exists in the elementary excitation spectrum of a superconductor. Thus, for a spinless superconductor (like a p-wave supercondcutor in 1D), the creation and annihilation operators of a Bogoliubov quasiparticle satisfy the relation $\Gamma_E^\dagger = \Gamma_{-E}$. Similar to the topological insulators, the different classes of BdG Hamiltonian preserving the particle-hole symmetry constraint that can be smoothly deformed without closing the superconducting energy gap can be distinguished topologically [56].

The fascinating consequence is the possible existence of topologically protected non-trivial edge states at the boundaries of spinless superconductors [57]. If an edge state were to appear within the energy gap say, with energy E, by particle-hole symmetry there exists a state at energy $-E$. Hence the bound states occur in finite energy pairs and can be pushed out of the gap into the bulk much alike the case of an even number of Kramers pairs, re-

Table 4.1: Topological periodic table

CLASS	TRS	PHS	SLS	*d=1*	*d=2*	*d=3*
A	0	0	0	-	$\mathbb{Z}$	-
AI	+1	0	0	-	-	-
AII	-1	0	0	-	$\mathbb{Z}_2$	$\mathbb{Z}_2$
AIII	0	0	1	$\mathbb{Z}$	-	$\mathbb{Z}$
BDI	+1	+1	1	$\mathbb{Z}$	-	-
CII	-1	- 1	1	$\mathbb{Z}$	-	$\mathbb{Z}_2$
D	0	+1	0	$\mathbb{Z}_2$	$\mathbb{Z}$	-
C	0	-1	0	-	$\mathbb{Z}$	-
DIII	-1	+1	1	$\mathbb{Z}_2$	$\mathbb{Z}_2$	$\mathbb{Z}$
CI	+1	-1	1	-	-	$\mathbb{Z}$

sulting in a trivial state. However, the bound state at $E = 0$ is evidently *unpaired* and cannot be eliminated, resulting in a topologically non-trivial state [57]. These two different states are distinguished by the $\mathbb{Z}_2$ topological invariant of the bulk superconductor.

In fact, a $\mathcal{T}$ invariant topological superconductor is nothing but a topological insulator with an additional particle-hole symmetry and is classified similarly by a topological invariant $\mathbb{Z}_2$ in 1D and 2D, and by $\mathbb{Z}$ invariant in the case of 3D (shaded violet in Table 4.1) [52]. Topological superconductors can also be differentiated based on $\mathcal{T}$ symmetry, the ones breaking the time-reversal symmetry are analogous to the integer quantum Hall state and give rise to chiral edge states, while those superconductors that are time-reversal invariant are analogous to the quantum spin Hall state resulting in helical superconductors. In the former case, an integer similar to the Chern number is used to classify the time-reversal breaking topological superconductors. The classification of topological insulators and topological superconductors into various classes and their topological invariants can be learnt from the topological periodic table in 4.1 where TRS is time-reversal symmetry, PHS is particle-hole symmetry and SLS is sublattice (or "chiral") symmetry. The presence (absence) of these symmetries is labelled either by "+" or "-" ("0"), depending on whether the eigenvalue of the corresponding squared antiunitary operator is +1 or -1. The first six rows represent non-superconducting systems while the last four represent superconducting systems [56].

The simplest model of a $\mathcal{T}$ breaking chiral topological superconductor in 2D can be realized in a p-wave pairing spinless superconductor [58] with a topological invariant $\mathbb{Z}_2$ belonging to Class D (see Table 4.1). In an s-wave paired superconductor, the ground state consists of a Bose condensate when there is strong attractive interaction and when the particles are weakly interacting, it consists of a quasiparticle excitation spectrum [58][23]. While there is no phase transition as we move from a strong pairing to a weak pairing

regime in a normal s-wave superconductor, it is not the same in case of a p-wave pairing superconductor where a phase transition does occur between the two regimes. This transition is of topological in nature as described by Volovik [55]. A spinless p-wave pairing state therefore has two distinct phases, a weak paring phase and a strong pairing phase corresponding to a topologically non-trivial phase and topologically trivial phase. The two phases are distinguished by a topological invariant and separated by a topological phase transition [58]. The intriguing property of the time-reversal breaking topological superconductors is that the Bogoliubov quasiparticle excitations occurring in these systems at zero energy are Majorana fermions that obey non-abelian statistics [59][60]. In order to understand the appearance of these exotic boundary states, a first look on the elusive Majorana fermions becomes essential.

4.3.1 Majorana fermions

Majorana fermions were first surmised by Ettore Majorana in 1937. Majorana fermions are particles that are their own anti-particles unlike the Dirac fermions such as electrons and positrons. The proposition that neutrinos may in fact be Majorana fermions still remains a mystery. It could be established if the neutrinos are found to violate lepton number conservation. Experiments at the Large Hadron Collider [61] and processes that involve neutrinoless double β decay [62] are being carried out to confirm the same, still, however, without a success. While particle physicists search for the mysterious Majorana fermion as fundamental particles of nature, Majorana fermions emerge as non-fundamental low-energy excitations in condensed matter systems.

Since a Majorana fermion is its own anti-particle, the creation and annihilation operators are equal, $\gamma = \gamma^\dagger$, with the property $\gamma^2 = 1$. But since particles and holes have opposite charges, being created by creation ($c_\sigma^\dagger$) and annihilation operators (c_σ) respectively, a Majorana fermion - with its creation and annihilation operator being equal - must necessarily be uncharged [63]. While the Bogoliubov quasiparticle in a superconductor possesses the necessary electron-hole superposition violating the charge conservation, the s-wave pairing observed in ordinary superconductors implies that the electrons and holes carry opposite spin projections. In an s-wave superconductor, the creation and annihilation operator of the Bogoliubov quasiparticles are of the form $b = uc_\uparrow^\dagger + uc_\downarrow$ and $b^\dagger = u^* c_\uparrow^\dagger + u^* c_\downarrow$, which are still physically distinct. For the particles to be Majorana fermions, they also need to possess equal spin projections. Thus to observe quasiparticles that are Majorana fermions, the ideal candidates are effectively spinless superconductors that involve Cooper pairs of the same spin ($s = 1$) with triplet pairing symme-

try [60]. As fermions obey antisymmetric exchange, in order to preserve the antisymmetry of the total wavefunction, a spin triplet state requires the symmetric orbital wave function be of odd parity ($l = 1, 3...$), the simplest case being p-wave ($l = 1$).

Majorana fermions therefore are expected to appear at the edges of p-wave superconductors in 1D, in the vortices of $p + ip$ superconductors in 2D, in Sr_2RuO_4 superconductor [64] which has triplet pairing and also in the $\nu = 5/2$ fractional quantum Hall state [65]. One of the breakthroughs in the prediction of Majorana fermions is when Fu and Kane [57] showed that zero-energy Majorana fermion modes can also appear at the interface between an ordinary s-wave superconductor and a topological insulator. The resulting surface states at the interface exhibits p-wave like pairing as a result of proximity effect. The work by Fu and Kane inspired other designs for achieving low-dimensional topological superconductors through a simple recipe involving spin-orbit coupling, s-wave superconductivity and magnetism in 2D structures [52]. Artificial engineering of p-wave superconductors from hybrid structures becomes a necessity as naturally occurring p-wave superconductors are hard to come by in nature. Before delving into the practical details of the realization of Majorana modes in proximity induced p-wave superconductors, it is crucial to look into the properties of Majorana fermions and the emergence of non-abelian statistics in these systems.

Properties of Majorana fermions

It is evident as to why the Bogoliubov quasiparticle excitations at zero energy modes in topological superconductors are Majorana fermions, they simply satisfy $\Gamma_0^\dagger = \Gamma_0$ at $E = 0$. A Bogoliubov quasiparticle at finite energy pair states E and $-E$ has the same physical degrees of freedom, implying that Majorana states at $E = 0$ possess half the degrees of freedom. Thus, a Majorana fermion is half of a Dirac fermion and a fermionic operator is constructed from a pair of Majorana fermions as

$$\begin{aligned} c_j &= (\gamma_{1,j} + i\gamma_{2,j})/\sqrt{2}, \\ c_j^\dagger &= (\gamma_{1,j} - i\gamma_{2,j})/\sqrt{2}. \end{aligned} \tag{4.4}$$

The fermionic operator constructed above still satisfies $c_j \neq c_j^\dagger$, while the Majorana fermions are hermitian $\gamma_j = \gamma_j^\dagger$ and obey the fermionic anti-commutation relations

$$\{\gamma_i, \gamma_j\} = 2\delta_{ij}. \tag{4.5}$$

Since a Majorana fermion is its own anti-particle, it is meaningless to regard a Majorana state being occupied or unoccupied. The occupancy of a Majorana

mode cannot be defined, even counting in terms of the number operator proves meaningless, $n_j^{mf} = \gamma_j^\dagger \gamma_j$ which by way of hermiticity is always $n_j^{mf} = \gamma_j^2 = 1$. However the fermionic state constructed from (4.4) can be occupied or empty and is physically meaningful. The number operator is defined as $n_j = c_j^\dagger c_j$ which by way of Pauli's exclusion principle is either $n_j = 0$ or 1. As a pair of Majorana fermions is combined together to form a fermion, $2N$ Majorana modes give rise to N number of fermionic states which can be either occupied or unoccupied leading to 2^N fold degenerate ground states. Moreover the eigenstates of the system can be defined in terms of the fermion number operator as $|n_1, n_2, ..., n_N\rangle$, while the sum of occupation numbers $\sum_{j=1}^{N} n_j$ gives the parity of the superconductor indicating the total number of electrons present. In conclusion, the *occupation numbers* n_j of electrons are the proper observables and not the occupation numbers of Majorana fermions [63].

Non-abelian statistics

In two-dimensional systems, quasiparticles that obey abelian statistics are referred to as abelian anyons while those which obey non-abelian exchange statistics and are non-commutative, are called non-abelian anyons. In a many-particle system, when identical particles undergo exchange, one particle goes through the other in loops or intersects their trajectories clockwise or counter-clockwise. A braid group consists of a map of the trajectories of the particles as they move from initial to final positions [66]. The transformation of the many-particle wavefunctions under these exchanges are given by the braid group acting on the states of the system. In case of an abelian braiding, wavefunctions of the particles remain in the same state but acquire a phase $e^{i\theta}$. If $\theta = \pi$ for a phase of -1, Fermi-Dirac statistics is recovered and for a value of 1, i.e. for a phase of $\theta = 0(2\pi)$, the particles are bosons and Bose-Einstein statistics is recovered. For other values of phase θ, the anyons are simply regarded to follow statistics θ [67]. Thus, quasiparticles that follow abelian statistics acquire a phase factor during an exchange that reflects the statistics they follow.

Non-abelian anyons are quasiparticles that do not acquire a phase factor under wavefunction exchanges but rather change to a *fundamentally different quantum state* [23]. As a consequence, the exchange process is noncommutative, thus the notion of *non-abelian statistics*. This is only possible when different quantum states of the system are degenerate. The system starts from an initial state and, as a result of the exchange, ends up in a different final state in the space of degenerate ground states. As the zero-energy Majorana modes of a topological superconductor are degenerate and robust

against perturbations, their topological degeneracy provides for non-abelian exchange statistics. Non-abelian statistics is known to occur in certain fractional quantum Hall states by virtue of the topological degeneracy of the quasiparticles [68][65]. It was established that a spinless p-wave superconductor in the weak pairing state behaves the same as that of a Moore-Read Pfaffian quantum Hall state and hence possesses similar properties of non-abelian statistics [58].

For a better comprehension of how the non-abelian statistics plays out, consider a 2D topological insulator with vortices hosting Majorana modes in their vortex cores. If the fermion number operator $n_j = c_j^\dagger c_j$ is deconstructed in terms of the Majorana operators from (4.4), then we get $n_j = c_j^\dagger c_j = (\frac{1}{2} + i\gamma_{1,j}\gamma_{2,j})$, two Majorana modes associated with one fermionic mode. When a pair of vortices are exchanged, the positions of the Majorana modes are also exchanged and the wavefunction is unitarily transformed within the degenerate ground state space and the resulting braid operator does not commute leading to non-abelian statistics [63]. Though the swapping of Majorana modes changes the fermionic state, the value of the number operator, n_j, remains the same which gives the total parity of the superconductor. A detailed description on the braiding operators governing the exchange of Majorana fermions and their non-abelian nature can be found in [63].

Topological quantum computation

Two Majorana modes defining a fermionic operator need not be local and can be spatially far apart from each other ensuing in a highly non-local fermionic state. A 'qubit' of quantum information can be stored in this highly non-local fermionic state. As non-abelian anyons - i.e. many-quasiparticle states with a topological degeneracy - are robust against local perturbations, quantum information stored in such systems [69] will also be robust and immune to errors caused by such perturbations, leading to fault-tolerant topological quantum computation [24]. A topological qubit is then encoded in the two-fold degenerate ground state represented by the number operator n_j. Since the degenerate ground state is separated from the bulk spectrum by an energy gap, if the manipulations on the qubit are carried out at sufficiently low temperatures, then the evolution of the system happens within the ground state manifold which remains unperturbed and not easily prone to decoherence. The obstacles faced with storing and processing quantum information, the methods of error corrections employed, and a detailed overview of topological quantum computation can be obtained from [66].

Therefore, superconductors hosting zero-energy Majorana fermion modes,

being non-abelian quasiparticles, serve as a viable platforms for carrying out fault-tolerant topological quantum computation.

While several experimental research groups have reported observations of signatures of Majorana fermions in topological superconductors [70][71] [72][73][74], further experimental studies are yet to be done to confirm their properties and their potential application in quantum computing. Majorana fermions have also been predicted to occur in cold atomic gases [75][76], in carbon nanotubes [77][78][79], in the vortices of doped topological insulators [80], and in B phase ^3He [60].

4.4 Theoretical model of Topological Superconductors supporting Majorana modes

The paradigm theoretical model describing the emergence of Majorana modes in a topological superconductor is the 1D toy model developed by Kitaev [22]. This simple set-up describes how *isolated* Majorana modes can be observed in a one-dimensional system. Consider a one-dimensional superconducting quantum wire consisting of a tight-binding chain of electrons with a fixed spin say, spin up ($\uparrow$), thus effectively spinless as required for realizing Majorana fermion states. The Hamiltonian of this 1D spinless p-wave superconductor can be described as

$$H = -t\sum_{j=0}^{N-1}(c_j^\dagger c_{j+1} + c_{j+1}^\dagger c_j) - \sum_{j=0}^{N-1}(\Delta^* c_j^\dagger c_{j+1}^\dagger + \Delta c_{j+1} c_j) - \mu\sum_{j=0}^{N} c_j^\dagger c_j. \quad (4.6)$$

Here c_j and $c_j^\dagger$ is the fermionic annihilation and creation operator respectively, μ is the chemical potential associated with the number operator, t is the hopping amplitude and $\Delta = |\Delta|e^{i\phi}$ is the superconducting gap induced due to p-wave pairing. ϕ is the superconducting pairing phase and can be absorbed into the fermionic operators defined in terms of Majorana fermion operators,

$$\begin{aligned} c_j &= e^{-i\phi/2}(\gamma_{1,j} + i\gamma_{2,j})/\sqrt{2}, \\ c_j^\dagger &= e^{i\phi/2}(\gamma_{1,j} - i\gamma_{2,j})/\sqrt{2}. \end{aligned} \quad (4.7)$$

From above, it is evident that Majorana fermions can be obtained by splitting the fermions into real and imaginary parts. Hence,

$$\begin{aligned} \gamma_{1,j} &= (e^{-i\phi/2}c_j^\dagger + e^{i\phi/2}c_j)/\sqrt{2}, \\ \gamma_{2,j} &= i(e^{-i\phi/2}c_j^\dagger - e^{i\phi/2}c_j)/\sqrt{2}. \end{aligned} \quad (4.8)$$

Thus $\gamma_{i,j}$ is the Majorana operator residing at site j. As two Majorana fermions are required for constructing a fermion, $j = (1, 2)$ indicates the two Majoranas (at 1 and 2) combining to form a fermion at site j. Clearly the above operators (4.8) are hermitian and obey the Majorana fermion relations (4.5). It can be seen that the fermionic operators are defined similar to (4.4) except for an additional phase ϕ. Now the Hamiltonian (4.6) is simplified to

$$H = -t\sum_{j=0}^{N-1}(c_j^\dagger c_{j+1} + c_{j+1}^\dagger c_j) - |\Delta|\sum_{j=0}^{N-1}(c_j^\dagger c_{j+1}^\dagger + c_{j+1}c_j) - \mu\sum_{j=0}^{N} c_j^\dagger c_j. \quad (4.9)$$

The newly defined fermionic operators (4.7) applied to the above Hamiltonian gives the Hamiltonian of a 1D spinless chain of p-wave paired electrons in terms of Majorana fermion operators,

$$H = i\sum_{j=0}^{N-1}[(t-|\Delta|)\gamma_{2,j+1}\gamma_{1,j} - (t+|\Delta|)\gamma_{1,j+1}\gamma_{2,j}] - \mu\sum_{j=0}^{N}(\frac{1}{2} + i\gamma_{1,j}\gamma_{2,j}). \quad (4.10)$$

There are two cases to consider here but an understanding of the nature of a spinless 1D chain and its bulk properties is required in prior. It should be noted that the time-reveral symmetry is broken as the spin is fixed in one direction. As previously mentioned, the spinless p-wave pairing has two phases, the weak-pairing phase and the strong-pairing phase distinguished topologically [55]. The Hamiltonian of a spinless electron system in the BCS mean field theory is written as,

$$H_{eff} = \sum_k[(\epsilon_k - \mu)c_k^\dagger c_k + \frac{1}{2}(\triangle_k^* c_k^\dagger c_{-k}^\dagger + \triangle_k c_{-k}c_k)]. \quad (4.11)$$

Here ϵ_k is the kinetic energy and $\triangle_k$ is the pairing amplitude. By applying perioduc boundary conditions to the above Hamiltonian, the BCS mean field equations and dispersion relations obtained show that the system admits a gapless phase at $\mu \to 0$, while $\mu > 0$ ($\mu < 0$) the system enters the weak-pairing (strong-pairing) phase [58]. Thus, a weak-strong topological transition occurs at $\mu = 0$. These two states can not only be distinguished topologically but also by the occupation number of their ground states. In the strong-pairing phase, as the name suggests, the Cooper pairs are tightly bound to each other and the energy required to break the pair becomes large, leaving the paired ground state to be unoccupied with an even number of fermions. In the weak-pairing phase, the topologically non-trivial phase, the Cooper pairs are not strongly bound to each other, with wavefunctions which now exhibit long-range behaviour. Hence, not much energy is required

to occupy a state or creating a quasiparticle in the ground state, leading to an odd number of fermions in the ground state. The system is gapped in both the cases.

Though the topologically non-trivial weak-pairing phase seems intriguing, what is more fascinating is the ground state at the transition $\mu = 0$, being degenerate between the occupied and unoccupied ground states. This is evident as a quasiparticle cannot simultaneously occupy both the single-particle states of the paired ground state, k and $-k$ at $k = 0$. Thus a degeneracy exists at $k = 0$ with occupied and unoccupied states. Therefore the system at the phase-transition point $\mu = 0$ supports two-fold degenerate ground states with even and odd number of particles [58]. Notably, adding an odd number of quasiparticles does not require any additional energy as the states of even and odd particles are degenerate. Whereas a conventional superconductor is non-degenerate and the ground state only supports Cooper pairs with even number of electrons. Adding an electron here costs non-zero energy.

Given these observations, we shall treat the Hamiltonian(4.10) following two special cases, the trivial case of strong-pairing where $\mu < 0$ and the non-trivial case for $\mu = 0$ at which the system undergoes a transition to the weak-pairing phase.

1 **The trivial case:** $\mu < 0$ and $t = |\Delta| = 0$. Then (4.10) becomes

$$H = -\mu \sum_{i=0}^{N} (\frac{1}{2} + i\gamma_{1,j}\gamma_{2,j}). \tag{4.12}$$

Clearly the Majorana operators coupled together belong to the same physical site j, evident from (4.7). There is an even number of fermions present in the ground state of the 1D chain and adding a single electron costs a finite energy $|\mu|$. The superconducting gap is preserved in this trivial strong-pairing phase.

2 **The non-trivial case:** $\mu = 0$ and $t = |\Delta| \neq 0$. Then (4.10) becomes

$$H = -2it \sum_{i=0}^{N-1} (\gamma_{1,j+1}\gamma_{2,j}). \tag{4.13}$$

The Hamiltonian here pairs up Majorana operators belonging to physically different sites j and $j + 1$. Now by defining new fermionic operators $d_i = (\gamma_{2,j} + i\gamma_{1,j+1})/\sqrt{2}$ and $d_i^\dagger = (\gamma_{2,j} - i\gamma_{1,j+1})/\sqrt{2}$ that couple the Majoranas belonging to neighbouring local sites j and $j + 1$, the Hamiltonian (4.13)

becomes

$$H = 2t \sum_{i=0}^{N-1} (d_i^\dagger d_i - \frac{1}{2}). \tag{4.14}$$

Similar to the previous case, the gap in the bulk of the system remains preserved and the cost of adding a fermion is 2t as seen above. The Hamiltonian (4.14) is not very different from (4.12) and has only been rewritten in terms of fermionic states obtained by superposition of Majorana fermion states of nearest-neighbour sites. The two ways of pairing Majoranas, pertaining to the Hamiltonians in (4.12) and (4.13), are illustrated in Figure 4.6 (a) and 4.6 (b) respectively.

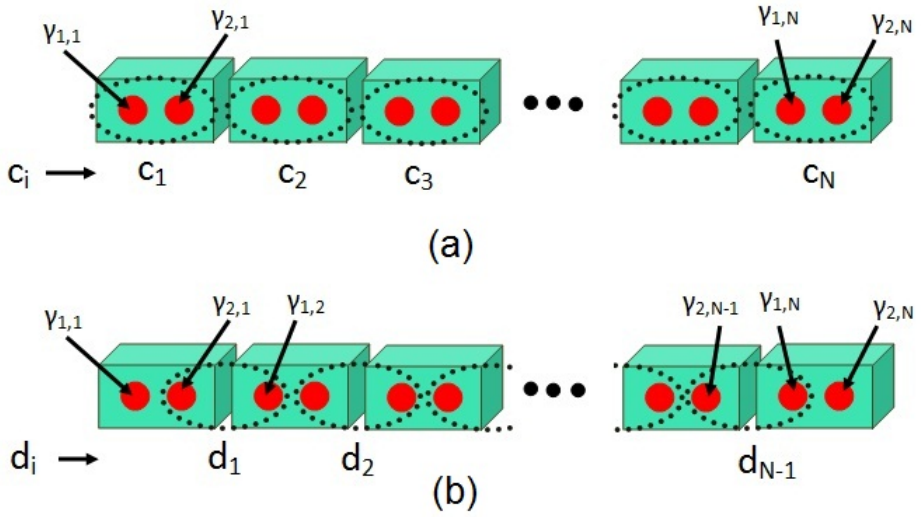

Figure 4.6: Kitaev's 1D spinless tight binding chain. (a) Trivial case in the limit of $\mu \neq 0, t = \Delta = 0$ where the Majoranas at the same lattice site are paired up to form a fermion. (b) Non-trivial case in the limit of $\mu = 0, t = \Delta$ where the Majoranas at the nearest-neighbour site are coupled together to represent a fermionic state [63]. Dotted lines depict the fermionic states formed by combining two Majorana states. Note: unpaired Majorana states $\gamma_{1,1}$ and $\gamma_{2,N}$ at the ends of the 1D chain.

The remarkable outcome of the non-trivial case above is that when observed carefully, one notices that the Majorana modes $\gamma_{1,1}$ and $\gamma_{2,N}$ are missing from the Hamiltonian (4.13). These two unpaired Majorana fermions present at the ends of this 1D spinless chain of electrons can be combined to form a single fermionic state with operator,

$$c_m = (\gamma_{1,1} + i\gamma_{2,N})/\sqrt{2}. \tag{4.15}$$

This fermionic state is highly non-local as the Majorana modes defining the fermionic operator are localized at the far ends of the 1D chain. The energy required to add or remove this fermion is *zero* and the ground state gives rise to a two-fold degeneracy. The two ground states $c_m |0\rangle = 0$ and $c_m^\dagger |0\rangle = |1\rangle$ with even and odd parity respectively, are degenerate.

At the transition, where the 1D chain goes from topologically non-trivial weak-pairing phase to topologically trivial strong-pairing phase, gapless edge states with zero-energy Majorana fermion states appear at the boundary between these two phases. It is not surprising why these gapless edge states occur at the ends of the 1D chain. In the topologically non-trivial phase with odd parity, the non-local fermion exists due to the presence of unpaired Majorana states, Figure 4.6(b). To turn this into a trivial phase with even parity, all one needs to do is but add a few more sites to the chain so that the unpaired Majorana states so that they are paired up to a fermion as in Figure 4.6(a). Thus it is at the ends of the 1D chain the transition between two distinct topological phases occurs. As these phases are topologically distinct, they cannot be smoothly deformed into one another and the bulk energy gap closes at the boundaries, i.e. at the ends of the 1D chain. It is important to add that additional Majorana fermion modes may appear if there is a defect along the wire which can host the Majoranas.

The appearance of zero-energy Majorana modes at the ends of the 1D chain is treated for the special case of $\mu = 0$. The Majorana end states continue to reside at the ends of the 1D chain as long as the system remains in the topologically non-trivial phase $\mu > 0$. In general for any $\mu \neq 0$ and $t \neq \Delta$, no zero modes exist for the case of $|\mu| > 2t$ which is the trivial phase of strong-pairing as in (4.12) with even parity and unpaired Majorana fermion modes exist for $|\mu| < 2t$, the topologically non-trivial phase with odd parity [22]. Additional Majorana fermion modes occur at points of phase transition called for by the change in chemical potential and hopping amplitude to $|\mu| > 2t$ along the wire [81]. In the case of topologically non-trivial weak-pairing phase, the unpaired Majorana modes are not just localized at the ends, their wavefunctions decay exponentially well into the chain and start overlapping. The interaction between the Majorana modes localized at the ends i.e. the wavefunction overlap is given by $w \propto e^{-L/\xi}$, where L is the length of the chain and ξ is the coherence length. If the chain is sufficiently long, for $L \gg \xi$, the wavefunction overlap is negligible and the ground state remains degenerate with unpaired Majorana modes localized to the ends. Otherwise, the wavefunction overlap causes a splitting of the even and odd degenerate ground states with $|0\rangle$ and $|1\rangle$ now differing by an energy w [23]. For the trivial case, ξ diverges. The factor w gains physical significance as it gives the amplitude of tunneling of a fermionic quasiparticle across the

chain [22]. The tunneling of an electron through the chain is viewed by way of coupling the Majorana fermion pair of the incoming electron with the unpaired Majorana zero-mode at the end of the chain.

To summarize our discussion, zero-energy Majorana modes are supported at the ends of the 1D spinless p-wave chain of fermions in Kitaev's toy model. If one considers a $\mathcal{T}$ invariant p-wave superconductor, a spinful chain, the fermions with spin up are paired together in a spin-up state and fermions with down spin together form a spin-down state. As a result, the edge states are merely doubled, with two Majorana zero-modes at the ends resulting in zero-energy Dirac fermion modes at the end.

In 2D, Majorana fermion modes appear at the vortices of a chiral $p + ip$ superconductor [58][59][82]. In $\mathcal{T}$ invariant helical superconductors, up spins are paired in $p_x + ip_y$ state and down spins in $p_x - ip_y$ state, giving rise to helical edge states [23]. Surprisingly, a 2D spinful $p_x \pm ip_y$ superconducting chain also supports isolated Majorana fermion states bound to *half quantum vortices* [59].

4.5 Realization of a Topological Superconductor supporting Majorana modes

One of the ways to realize a topological superconductor is by inducing superconductivity through proximity effect in a topological insulator [57]. These topological superconducting states host Majorana fermion modes at the edge states in 2D and at the surface states in the case of 3D. A 2D topological insulator is TR invariant and consequently these topological superconducting states preserve time-reversal symmetry giving rise to a pair of helical edge states, i.e. Majorana Kramers pairs with the opposite spins moving in counter-propagating directions along the edges. One can also engineer a topological superconductor by replacing a topological insulator with a semiconductor provided the material has appreciable spin-orbit coupling [81][83]. In short, the essential ingredients required to realize a 1D spinless p-wave superconductor using a semiconductor are, (i) a semiconducting wire with *strong spin-orbit coupling*, (ii) a magnetic field that *breaks time-reversal symmetry*, and (iii) a conventional s-wave superconductor to induce *proximity effect*.

Thus, let us consider a set-up with a 1D nanowire with strong spin-orbit coupling such as InAs or InSb, coupled to a bulk s-wave superconductor such as Nb, exposed to an external magnetic field. See Figure 4.7. Such a 1D wire is represented by a Hamiltonian of the form

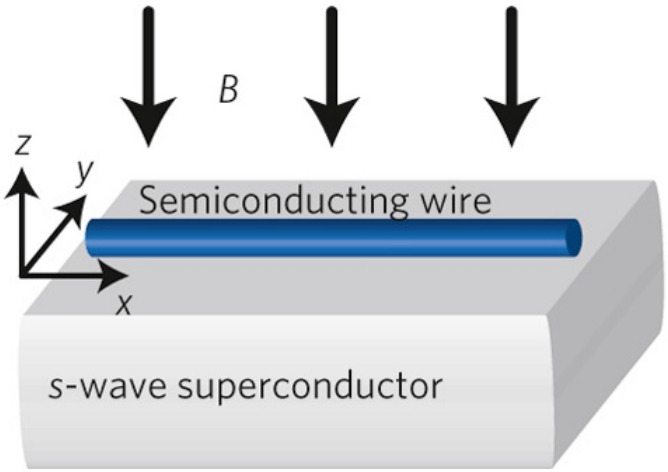

Figure 4.7: Set-up for realization of a 1D spinless p-wave superconductor [23].

$$H_{wire} = \int \psi_\sigma^\dagger \mathcal{H}_{wire}(x) \psi_\sigma \, \mathrm{d}x, \tag{4.16}$$

$$\mathcal{H}_{wire}(x) = \frac{k_x^2}{2m} - \mu + \alpha k_x \sigma^y + h\sigma^z. \tag{4.17}$$

Taking $\hbar = 1$, m is the effective mass of the electron, μ is the chemical potential of the wire, α is the strength of spin-orbit interaction due to Rashba spin-orbit coupling in the wire along the y-direction, and h is the strength of the Zeeman field due to the magnetic field applied along the z-direction.

The 1D semiconducting nanowire proximity-coupled to a conventional s-wave superconductor becomes superconducting as it acquires Cooper pairing from the parent superconductor. The Hamiltonian describing the process can be written as

$$H_\Delta = \int \Delta(\psi_\uparrow \psi_\downarrow + h.c) \, \mathrm{d}x, \tag{4.18}$$

where Δ is the pairing amplitude. Thus, the total effective Hamiltonian to be considered is,

$$H_{eff} = H_{wire} + H_\Delta. \tag{4.19}$$

It is the external magnetic field and the spin-orbit coupling that together conspire in such a way as to transform s-wave proximity pairing into p-wave pairing. To understand the physics of this phenomenon in detail, let us consider the behaviour of the wire in (4.17) in the absence of superconducting

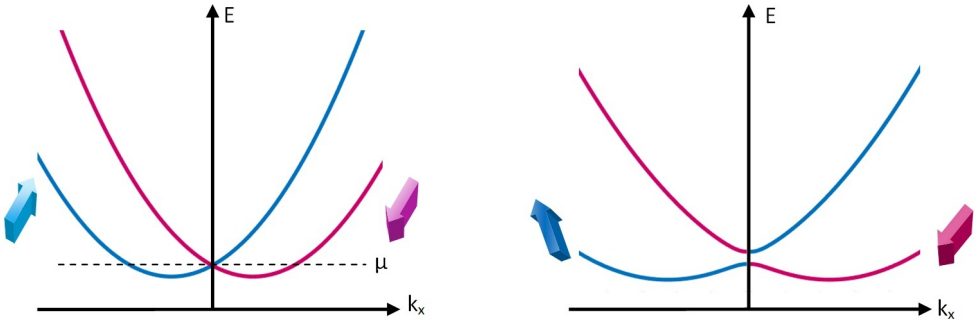

(a) (b)

Figure 4.8: (a) Eigenspectrum (4.20) of a 1D nanowire with spin-orbit coupling at $h = 0$. Blue and pink parabolas correspond to spins aligned along directions $-y$ and $+y$ (going in and out of the surface as indicated) respectively. (b) Band structure of the wire with a small applied magnetic field $h > 0$, resulting in a gap and loss of spin degeneracy at $k = 0$.

pairing field, i.e. with $\Delta = 0$. The spin-orbit split energy spectrum of H_{wire} in the absence of a magnetic field, $h = 0$ is sketched in Figure 4.4(a) with the Rashba coupling aligning the spins along the y-direction. As seen in Figure 4.8 (a), the spin degeneracy is lifted everywhere except at the Kramer's point $k = 0$. This last remaining degeneracy can be lifted by applying a magnetic field, which opens a gap in the spectrum as seen in Figure 4.8 (b). Diagonalizing the Hamiltonian (4.17), one obtains the eigenenergies as

$$E_{\pm}(k_x) = \frac{k_x}{2m} - \mu \pm \sqrt{(\alpha k_x)^2 + h^2}. \tag{4.20}$$

The band energies $E_+(k_x)$ and $E_-(k_x)$ correspond to upper and lower bands respectively. Usually, with Zeeman splitting, the bands consisting of either spin up or spin down states are separated by a gap. However, because spin-orbit coupling is also present, the lower band $E_-(k_x)$ consists of a mixture of spin up and spin down states as illustrated in Figure 4.8(b).

Thus, spin is no longer a good quantum number and effective spin direction in the band depends on the momentum along the direction x resulting in spin-momentum locking. The larger the applied field, the larger is the gap and the spin canting, causing spins within each band to align more in the z-direction as depicted in Figure 4.9(a). When the chemical potential μ lies inside such a field-induced gap, the wire emerges spinless and by turning on the superconducting pairing field, one induces spinless superconductivity in the wire. Figure 4.9(b) shows the canting of spins along the z-direction with respect to an increase in Zeeman energy h.

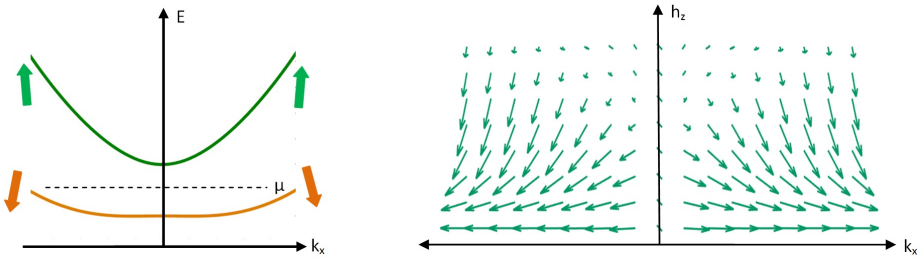

(a) (b)

Figure 4.9: (a) Energy bands under large magnetic field resulting in spinless electronic states . (b) Gradual canting/tilting of the spin in the lower band, with respect to increase in applied magnetic field, progressing towards a spinless regime where the spins are oriented parallel or anti-parallel to the field in z-direction.

Switching on the proximity-induced superconducting field $\Delta > 0$ only influences electrons occupying the lower band as the chemical potential μ resides in the gap and the upper band remains unoccupied. This leads to single-branch BCS pairing of electrons in the lower band, wherein the s-wave pairing field couples electrons with opposite spin directions. This leads to an effective spinless p-wave pairing since spin in the lower band has become a redundant degree of freedom, being locked to the momentum of the electron (Figure 4.9 (a)). Only a pairing field that is weak compared to the applied magnetic field $\Delta << h$ guarantees aforesaid *intra-band p-wave pairing* ensuing in a superconducting state that is topological [23]. Said topological superconducting state is associated with Majorana fermions and can be mapped to the weak-pairing phase of Kitaev's toy model.

If the chemical potential is large then the electrons begin to occupy the upper band and one cannot simply ignore the upper band as before. Also a larger pairing Δ gap not only leads to single branch BCS pairing but also causes inter-branch pairing akin to an FFLO state [84][85] where the Cooper pairs acquire a non-zero centre of mass momentum. Coupling of electrons in the upper and lower bands that carry opposite spin directions results in inter-band s-wave pairing in addition to the previously discussed intra-band p-wave pairing and when the former dominates the latter, the resulting superconducting state is no longer topological and the wire becomes a normal superconductor.

The phase transition between topological and trivial states can only arise when the gap closes. The gap closing and the associated topological criterion can be obtained by solving the Bogoliuobov de Gennes equations for the

Hamiltonian in (4.18) obtaining the quasiparticle energies for the superconducting wire (4.19) [63]. It is found that the gap in the quasiparticle energy spectrum closes exactly when the applied field is $h = \sqrt{\Delta^2 + \mu^2}$ [23]. As p-wave pairing occurs only when ($\Delta << h$), it is evident that the condition for topological superconductivity requires,

$$h > \sqrt{\Delta^2 + \mu^2}. \tag{4.21}$$

Having thus obtained a spinless p-wave superconducting wire, Kitaev's model predicts that it will host Majorana zero modes at its ends.

One can tune the various parameters to achieve a stable topological phase. Adding a set of gate electrodes can help control and vary the chemical potential such that it lies within the gap. Though a large magnetic field assures a topological superconducting state, a very large magnetic field makes the very topological state prone to disorder. Moreover, if the Zeeman energy h dominates the spin-orbit energy ($E_{so} = \frac{1}{2}m\alpha^2$), then the electrons may become completely spin polarized, making it impossible to induce superconductivity. See Figure 4.9(b) where the spins become fully aligned with increasing h. A small h/α ensures that the spins are not completely aligned. It assures proximity induced superconductivity, with the topological phase also being less susceptible to disorder. Thus, a large spin-orbit coupling α is essential for the topological phase to remain robust against perturbations [23]. With larger spin-orbit coupling, one has the freedom to play with the strength and direction of the magnetic field, increasing it in such a way that the Zeeman-split induced gap remains large enough to accommodate the chemical potential inside. If, however the pairing gap becomes larger, then the wire enters a normal superconducting state, the trivial one. In conclusion, to attain a stable robust topological phase, the Zeeman energy should be higher than the superconducting pairing energy but less than the spin-orbit energy, $\Delta << h << E_{so}$.

Thus, a simple setup involving a semiconducting nanowire with spin-orbit coupling, exposed to a magnetic field and in proximity to an s-wave superconductor realizes a topological superconductor. By optimizing the parameters, a robust topological phase is obtained. Moreover, the Majorana bound states localized at the ends of these topological superconductors are robust to perturbations, exhibiting topological degeneracy. Though signatures of Majorana fermions in 1D nanowires have been reported [70], their topological properties await further investigation as fabrication and measurement techniques pose a great challenge. If experimental ways were to attain reproducible realizations of Majorana modes, it would herald the study and demonstration of topological protection, and subsequently, in the long haul, topological quantum computation.

Chapter 5

Topological Kondo effect

While a topological superconductor achieved in a 1D nanowire hosts a pair of Majorana fermion modes each localized at its ends, the minimal set-up required to study the topological Kondo effect [1] requires four such Majorana end modes. Therefore, two 1D nanowires are placed on top of an island with a conventional parent bulk superconductor (see Figure 5.1). Once the wire enters the topological superconducting phase[1] , the superconducting island now supports four Majorana modes localized at the ends of the wires, three of which are connected to normal metal leads. The spinless conduction electrons on the island are now weakly coupled to these metal leads. Once this mesoscopic set-up is connected to ground by a capacitor, the finite charging energy of the superconducting island takes a crucial role in the investigation of Majorana fermion modes. If C is the total capacitance of the superconducting island, the bare charging energy is given by $E_c = \frac{e^2}{2C}$. It is the minimum energy required for tunneling into the system and no current flows at temperatures and voltages below E_c. The effective energy required to add N electrons to the superconducting island is governed by the bare charging energy term in the Hamiltonian, (5.1)

$$H_c = E_c\left(N - \frac{Q_g}{e}\right)^2. \tag{5.1}$$

Here $N = 2n_c$, 'n_c' being the total number of Cooper pairs on the island. Q_g is the gate charge due to the gate voltage V_g across the capacitor, and e is the electronic charge. With the bare charging energy setting the energy scale of the system, the effective charging energy gives the total electrostatic energy needed to charge the mesoscopic system with N electrons.

[1] supported by the combined action of a strong Rashba spin-orbit coupling and a transverse magnetic field, cf. the discussion in the previous chapter

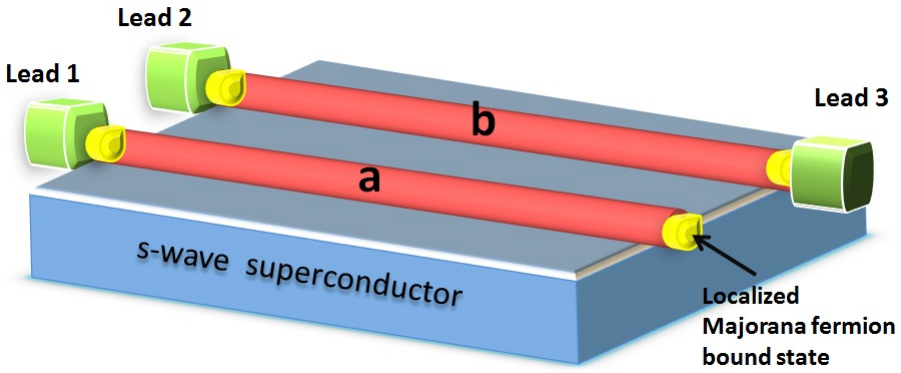

Figure 5.1: The topological Kondo effect set-up consists of two similar wires 'a' and 'b' (in pink) deposited on an s-wave superconductor. The ends of the wires are connected to three leads marked green and when they enter the topological phase, a total of four Majorana bound states are localized at the ends of the two wires (indicated by a yellow bubble).

5.1 Role of charging energy in the energy spectrum of a superconductor

An approach to understand the role of charging energy is by looking into the superconducting ground state. In a conventional superconductor the ground state consists of paired electron states, a.k.a. the Cooper pairs separated from the single-electron quasiparticle states by a superconducting energy gap. It does not require any energy to add a Cooper pair of charge $2e$, however, in order to add a single electron of charge e, an additional energy to overcome the superconducting pairing gap is needed such that the unpaired electron can occupy one of the quasiparticle states; cf. Figure 5.2(a). Therefore, to describe the ground state energy of the superconducting island with an added parity term Δ_N, the above equation (5.1) can be rewritten as

$$E_0(N) = E_c\left(N - \frac{Q_g}{e}\right)^2 + \Delta_N, \tag{5.2}$$

$$\Delta_N = \begin{cases} 0 & \text{when } N \text{ is even} \\ \Delta & \text{when } N \text{ is odd.} \end{cases} \tag{5.3}$$

The ground state is degenerate with paired (even number of electron) states, while the excited states consist of odd number of electron states, separated from the ground state by a gap. Nevertheless, in any system the ground state is degenerate only in the thermodynamic limit (as $N \to \infty$) with an

infinitely large system of particles, with the degenerate states being classified by a well-defined phase ϕ of the superconductor. Then the ground state is represented by a BCS wave function, $|BCS, \phi\rangle$, $\phi \in [0, 2\pi]$, with a coherent superposition of states with all possible Cooper pairs. But for a mesoscopic system with a finite number of particles, the ground state is non-degenerate due to finite-size effects [42]. Therefore, with the charging energy governing the addition of electrons to the superconducting island, it is evident from the expression in (5.2) that electronic states with varying N are non-degenerate. As portrayed in the energy spectrum of superconductor in Figure 5.2(b), the non-degenerate ground states of different number of electrons are still separated from odd states by an energy gap Δ.

However there exists a degeneracy between states $N-2$ and N (assuming N is even) when the gate charge, $\frac{Q_g}{e}$, is fixed such that it takes a value equal to $N-1$. With an increase in energy levels the next degeneracy point is attained between $N-4$ and $N+2$, as seen in Figure 5.3. This degeneracy is governed by the gate charge Q_g which in turn is controlled by the gate voltage and only for odd values, i.e. $\frac{Q_g}{e} = 2n_c - 1$, such degeneracy is observed (with n_c, the number of Cooper pairs). The effective charging energy $E_0(N)$ thus gets minimized to the bare, finite charging energy E_c by increasing the gate charge by $\frac{Q_g}{e} = 2n_c - 1$ lifting the Coulomb blockade. The number of excess Cooper pairs on the island is a staircase function of $\frac{Q_g}{e}$ which jumps at every $2n_c - 1$. Thus, an energy level degeneracy exists between two states which differ by an even number of electrons, and a superposition of these two states gives a coherent quantum state. In general, a degeneracy between states N and $N \pm 1$ can be obtained by changing the gate charge fraction to $\frac{Q_g}{e} = 2n_c \pm 1$. The superconducting island thus serves as a Cooper-pair box. This can be realized experimentally and allows coherent manipulation of its quantum state [86].

While the degenerate ground states in thermodynamic limit $N \to \infty$ is defined by a definite overall superconducting phase ϕ, the non-degenerate states with a well-defined particle number N has an indefinite phase. Thus, when fluctuations in Cooper-pair number are restricted, quantum fluctuations of the superconducting phase ϕ are large. It is possible to project out a definite N-particle state out of the usual BCS ground state using the method employed by P.W.Anderson [87] by integrating the many-particle ground state over all values of ϕ such that

$$|BCS, N\rangle = \int_0^{2\pi} e^{-i\phi N/2} \, |BCS, \phi\rangle \, \mathrm{d}\phi. \tag{5.4}$$

From the above equation (5.4), one succeeds in obtaining states with a precise particle number N (N must be even as the wavefunction includes only pairs).

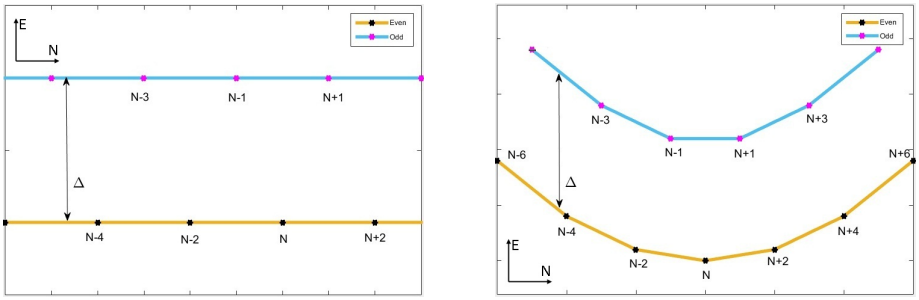

(a) (b)

Figure 5.2: Energy spectrum of a superconductor (a) without charging energy, (b) with charging energy, both with a pairing energy Δ.

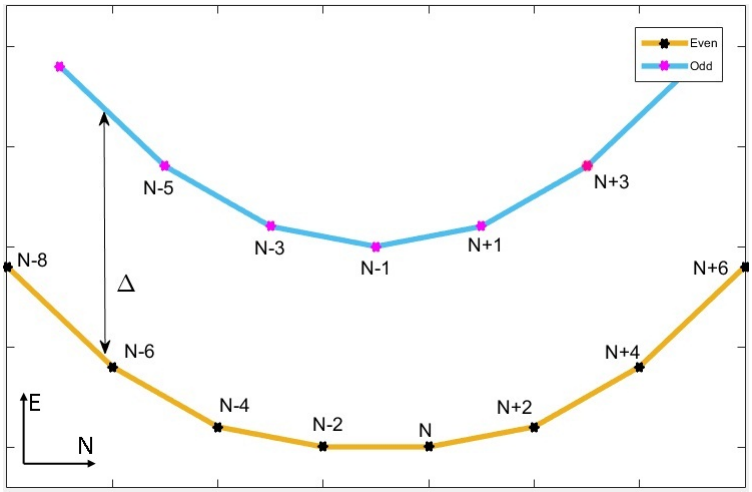

Figure 5.3: Energy spectrum of a superconductor with charging energy exhibiting energy-level degeneracy between states that differ by an even number of electrons (with charge $2e$,$4e$,.. etc.). Here the fraction of gate charge is fixed to $N-1$ ($2n_c-1$ in terms of Cooper pairs).

A Fourier transform of (5.4) yields a phase-number uncertainty relation [88]. Much alike the position $\hat{x}$ and momentum $\hat{p}$ operators, the superconducting phase and number of extra Cooper pairs on the island can be associated with conjugate quantum operators [42], $\hat{\phi}$ and $\hat{n}_c$, implying that

$$\begin{aligned} [\hat{n}_c, \hat{\phi}] &= -i, \\ \Delta n_c \Delta\phi &\geq \frac{1}{2}. \end{aligned} \tag{5.5}$$

The Hamiltonian in (5.1) remains unaltered in the discrete charge basis

representation and since the island has a definite number of Cooper pairs, $\hat{n_c}\,|n_c\rangle = n_c\,|n_c\rangle$, with $\hat{\phi} = i\partial/\partial n_c$, as follows from (5.5). From the phase-number uncertainty and the conjugation relation in (5.5), it can also be shown that [88] [89]

$$[\hat{n_c}, e^{\pm i\hat{\phi}}] = \pm e^{\pm i\hat{\phi}} \tag{5.6}$$

From this the effect of acting with $e^{\pm i\hat{\phi}}$ on the charge eigenstates can be inferred as

$$\begin{aligned} e^{i\hat{\phi}}\,|n_c\rangle &= |n_c + 1\rangle\,, \\ e^{-i\hat{\phi}}\,|n_c\rangle &= |n_c - 1\rangle\,. \end{aligned} \tag{5.7}$$

Thus, the operator $e^{i\hat{\phi}}$ raises the number of Cooper pairs on the island by 1, while the operator $e^{-i\hat{\phi}}$ removes a Cooper pair.

The significance of the charging energy falls into place with the number-phase uncertainty relation as it dictates whether the superconducting island behaves as a macroscopic quantum system or a mesoscopic quantum system. In a weakly coupled system, when the charging energy is large, it allows only a discrete transfer of charges $2e$ in exclusive Cooper pairs between the leads across the superconducting island. In the case of a small island, at most a single Cooper pair is transferred [86][90], thus operating in a well-defined charge regime, exhibiting Coulomb blockade. In contrast, a very small charging energy results in a coherent transfer of a macroscopic number of Cooper pairs across the island, causing large fluctuations in the Cooper-pair number resulting in macroscopic quantum tunneling, with the system functioning in a well-defined phase regime [91].

5.1.1 Superconductor with a pair of Majorana fermion bound states

The notions discussed hitherto do not take into account Majorana fermions and how the presence of Majorana fermion bound states modify the low-energy spectrum in the case of a topological superconductor. In the absence of Majorana fermions, the lowest branch of the spectrum of the superconductor only consists of even states, but with a pair of zero-energy Majorana bound states present, both even and odd states are possible. Since the unpaired zero-energy Majorana bound states localized at either ends of the wire forms a non-local fermion state, $c_m^\dagger = \gamma_1 + i\gamma_2$, there is no energy expense to occupy this state as it is not separated from the ground state by a finite energy gap. While it costs an energy equal to the pairing energy gap Δ to occupy an unpaired electron state in a normal superconductor as seen in

equation 5.2, it costs zero energy to occupy the unpaired electron state in a topological superconductor with zero-energy Majorana bound states. This single electron quasiparticle state can no longer be ignored. Therefore, the ground state illustrated in Figure 5.4(a) now includes both even and odd states. When n_m zero-energy Majorana fermion modes form $n_m/2$ fermion states that can be either occupied or empty, it results in a $2^{n_m/2}$-fold ground state degeneracy. However, parity of these Majorana states is related to the total parity of the superconducting island with N fermions and when the parity of the fermions is fixed, the resulting ground state exhibits $2^{(n_m/2)-1}$-fold degeneracy [23]. Thus, for any exotic effects to occur $n_m > 2$ is required, and ergo, the set-up of a topological Kondo effect consists of the minimal $n_m = 4$ Majorana zero modes (with $n_m = 3$ being excluded since n_m should be even) [1].

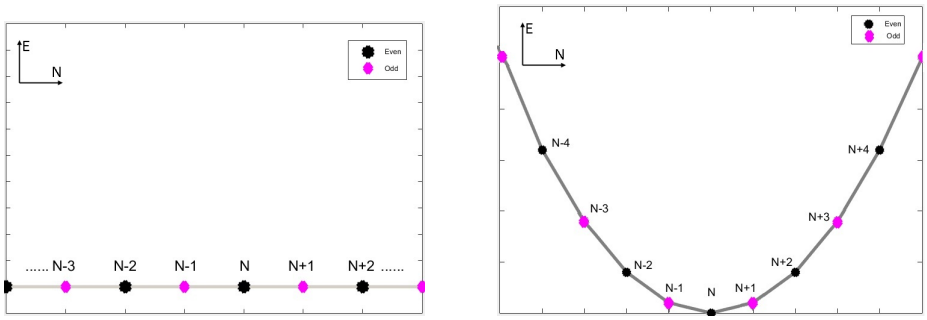

(a) (b)

Figure 5.4: Energy spectrum of a superconductor with a pair of zero-energy Majorana bound states (a) without charging energy, (b) with charging energy.

However, we have seen that for a system with finite charging energy, consisting of a well-defined number of particles, the ground state is non-degenerate and the energy spectrum with Majorana bound states now resembles that of the lowest branch of Figure 5.2(b) but now containing both even and odd states.

Parallel to the previous case, one can obtain a solution where both even and odd states are degenerate by carefully tuning the value of gate charge. The energy spectrum then exhibits degeneracy points whenever the gate charge fraction is adjusted to half integers $\frac{Q_g}{e} = N + \frac{1}{2}$ much alike the case of a single electron box. Thus, a superconductor with zero-energy Majorana fermion modes supports energy-level degeneracy between states that differ by odd number of charges rather than even number of charges. This non-local fermion state forms a two-level system in analogy to the single Cooper-pair

box. In the same way, it can be used to store quantum information with an added advantage of non-locality and topological protection.

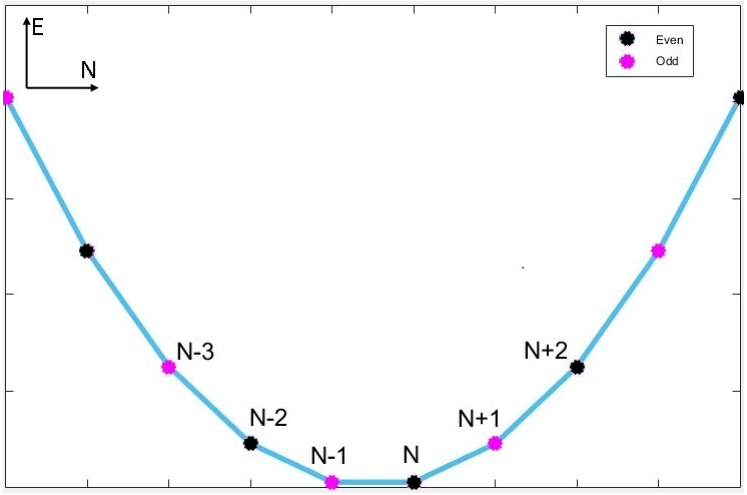

Figure 5.5: Energy spectrum of a superconductor with a pair of zero-energy Majorana fermion bound states exhibiting energy-level degeneracy between even and odd states that differ by odd number of charges (e,$3e$,.. etc.).

If a zero-energy Majorana bound state appears at a position R along the superconducting wire, then the quasiparticle operator of the Majorana fermion bound state takes the form

$$\gamma = \int [\xi_R(x) e^{-i\frac{\phi}{2}} \psi^\dagger(x) \; + \; \xi_R^*(x) e^{i\frac{\phi}{2}} \psi(x)] \mathrm{dx}, \tag{5.8}$$

where $\xi_R(x)$ is a bound state envelope function centred at R that falls off exponentially with distance and characterizes wavefunction overlap. However, the length of the wire is assumed to be larger than the coherence length such that Majorana modes localized at the ends of the wire have essentially zero wavefunction overlap, thus preserving the phenomenon of non-locality. $\psi^\dagger(x)$ and $\psi(x)$ are electron creation and annihilation operators.

5.2 Electron transport via Majorana bound states

Coupling the Majorana bound states to the metal leads makes it possible to tunnel single electrons through the non-local fermion state. The finite

charging energy of the system not only influences the energy spectrum of the superconducting island, but also impacts tunneling of electrons through the island. In a normal superconductor, tunneling of single electrons is impractical due to the pairing energy gap Δ for single-particle excitations and only Cooper pairs tunnel readily, resulting in a tunneling sensitive to parity with a periodicity of $2e$ [92]. For any applied bias voltage $V < E_C < \Delta$, quasiparticle excitations separated by a finite energy gap of Δ are unimportant and only zero-energy Majorana fermions become the main focus in tunneling. If the quasiparticle energy were less than the charging energy, $E_\Delta << E_C$, it will drastically alter the physics of the device, as the tunneling process via these quasiparticle states will compete with the tunneling of electrons through Majorana bound states, resulting in quasiparticle poisoning of the device [93]. Hence, for realizing a stable topological Kondo effect, it is important to have $E_C < \Delta$ in our present study.

The first step in recognizing tunneling of electrons from the leads to the superconductor is by defining the electron operators of the superconductor in terms of the Majorana fermion operators. Using (5.8) one has

$$\begin{aligned} \psi^\dagger(x) &= e^{i\frac{\phi}{2}}[\xi_i(x)\gamma_i^\dagger + \xi_j(x)\gamma_j^\dagger], \\ \psi(x) &= e^{-i\frac{\phi}{2}}[\xi_i(x)\gamma_i + \xi_j(x)\gamma_j]. \end{aligned} \tag{5.9}$$

The above expression is different from (4.7) as it includes a bound state wavefunction term associated with the Majorana fermions, and the significance of it becomes evident during tunneling. Here the Majorana wavefunction $\xi_i(x)$ and $\xi_j(x)$ denote the Majorana bound states localized at the ends of wire coupled to leads i and j respectively. As the Majorana wavefunction peaks at the point of contact and falls of exponentially with distance, $\xi_i(j)$ and $\xi_j(i)$ are zero.

A Majorana fermion is a superposition of a particle and a hole state, and it is a misconception to recognize it as a particle as it makes no physical sense with respect to being occupied or empty. One can wonder if a fermionic state formed by combinations of these Majorana fermions has any physical significance at all and doubt its occupancy. But it is the factor $e^{\pm i\phi/2}$ which comes to the rescue. Similar to the phase operators defined in (5.7), $e^{i\phi/2}$ adds an electron and $e^{-i\phi/2}$ removes an electron. Thus, an electron tunneling through the non-local fermion state appears as if it is being teleported since it enters the superconducting island through a Majorana bound state at one end and comes out of the Majorana bound state at the other end [94].

Consequently - an electron tunneling into superconducting wires a and b shown in Figure 5.1 is represented by similar operators as above. If 't_i' is

the tunneling probability of an electron hopping from a lead i (since only three leads are connected, i=1,2,3) into the superconducting island, then the effective Hamiltonian describing the transitions of electrons is obtained by second-order perturbation theory as

$$H_T = \sum_{i \neq j} \lambda_{ij}^{+} \gamma_i^{\dagger} \gamma_j \psi_j^{\dagger} \psi_i - \sum_j \lambda_{jj}^{-} \psi_j^{\dagger} \psi_j. \tag{5.10}$$

Here, $\lambda_{ij}^{\pm} = t_i t_j \left(\frac{1}{U_+} \pm \frac{1}{U_-} \right)$ and $U_{\pm} = E_0(N \pm 1) - E_0(N)$, see Appendix B for a detailed derivation. In [1], the effective tunneling Hamiltonian is obtained by a Schrieffer-Wolff transformation, but here we follow an alternative approach involving time-dependent perturbation theory to calculate the transition rates. The total Hamiltonian, including the leads, is given by, $H_{\text{eff}} = H_{\text{leads}} + H_T$. The Hamiltonian of the conduction electrons in the leads, H_{leads}, is assumed to be non-interacting for realization of topological Kondo effects [1]. Hence, Hamiltonian H_T with a finite charging energy E_c brings about a transition between states $|N\rangle$ and $|N \pm 1\rangle$ of the superconducting island, corresponding to even and odd states respectively.

5.3 Emergence of Kondo effect

The charge fluctuations between states $|N\rangle$ and $|N \pm 1\rangle$ in the superconducting island set-up leads to Coulomb blockade phenomenon which can be captured by a multichannel Kondo model. To arrive at the precise Kondo model, first the Majorana fermion operators in (5.10) are expressed in terms of spin-1/2 operators,

$$\sigma_1 \equiv i\gamma_2\gamma_3 \ , \sigma_2 \equiv i\gamma_1\gamma_3 \ , \sigma_3 \equiv -i\gamma_1\gamma_2. \tag{5.11}$$

These operators, by virtue of the fermionic anticommutation relations (4.5), obey the SU(2) spin algebra

$$[\sigma_i, \sigma_j] = i\varepsilon_{ijk}\sigma_k. \tag{5.12}$$

Now to attain a Kondo model from the tunneling Hamiltonian in (5.10), $H_T \rightarrow H_{\text{Kondo}}$, the electron operators in (5.10) are represented by a spin current J_α such that

$$J_\alpha = i \sum_{a,b} \varepsilon_{\alpha a b} \psi_a^{\dagger} \psi_b. \tag{5.13}$$

with a and b denoting the two wires and $\alpha = 1,\ 2,\ 3$ indicating the three leads coupled to the wire. Now on closer inspection one finds that J_α is

nothing but a spin-1 representation of electrons as

$$J_\alpha = i \sum_{a,b} \varepsilon_{\alpha ab} \psi_a^\dagger \psi_b \equiv \Psi^\dagger \mathcal{J}_\alpha \Psi. \tag{5.14}$$

Here $\mathcal{J}$ symbolizes the matrices representing spin-1 electrons, analogous to the Pauli matrices of spin-1/2 electrons, with Ψ serving as spin-1 electron operators. Therefore, the reformulation of the tunneling Hamiltonian, $H_T \to H_{\text{Kondo}}$, maps it to a spin-1/2 two-channel Kondo model with spin-1 conduction electrons,

$$H_{\text{Kondo}} = \frac{1}{2} \sum_\alpha \lambda_\alpha \sigma_\alpha J_\alpha, \tag{5.15}$$

where $\lambda_\alpha = \sum_{a,b} |\varepsilon_{\alpha ab}| \lambda_{ab}^+$. As mentioned above, the spin-1/2 impurity two-channel Kondo model of spin-1 conduction electrons is found to be equivalent to a spin-1/2 impurity four-channel Kondo model of spin-1/2 conduction electrons by way of their algebra, as both follow an $SU(2)_4$ Kac-Moody algebra [40].

It is evident why a minimal $M = 3$ coupling of leads is required as both the spin-1 impurity J_α and spin-1/2 conduction electrons represented by σ_α require 3 couplings in order to achieve the Kondo interaction in (5.15). When considered as a topological qubit, the σ_α operators serve as Pauli matrices [95]. Because the Kondo coupling λ_α should be set positive to realize antiferromagnetic interaction, the value of the charging energy has important consequence for the topological Kondo effect. The Kondo coupling term also includes the tunneling amplitudes t_i, which always remain positive with a proper choice of the phase of electron fields. The role of charging energy on the Kondo coupling term can be understood by expanding the term λ_{ij}^+, which results in

$$\lambda = \frac{2}{E_c \left[1 - 4 \left(N - \dfrac{Q_g}{e} \right)^2 \right]}. \tag{5.16}$$

The charging energy E_0 of the superconducting island is usually minimized to facilitate addition of electrons. While the gate charge is set to fractional values $\frac{Q_g}{e} = N + \frac{1}{2}$ to obtain an energy-level degeneracy between even-odd states and to achieve minimization of the charging energy, the fractional values cause a blow-up of the coupling strength as is evident from (5.16). For a positive λ the gate charge fraction should be minimized further such that it is less than $N + \frac{1}{2}$. The straightforward way is to set the gate charge fraction to be rather integers equal to N. Therefore, by tuning $\frac{Q_g}{e} = N$ ensures a positive antiferromagnetic Kondo coupling and also minimizes the

charging energy E_0 to the bare charging energy. The bare Kondo coupling strength is then $\sim 2/E_c$.

Since the signature of Majorana fermions is observed as zero-bias conductance peaks [70], the signature of the Kondo effect can be recognized by doing conductance measurements and studying its temperature dependence. While the Coulomb blockade suppresses the linear conductance at low temperatures, the Kondo effect enhances it. Therefore, an increase in conductance occurs and ceases when any one of the three leads is decoupled, serving as a smoking-gun signature of the Kondo effect.

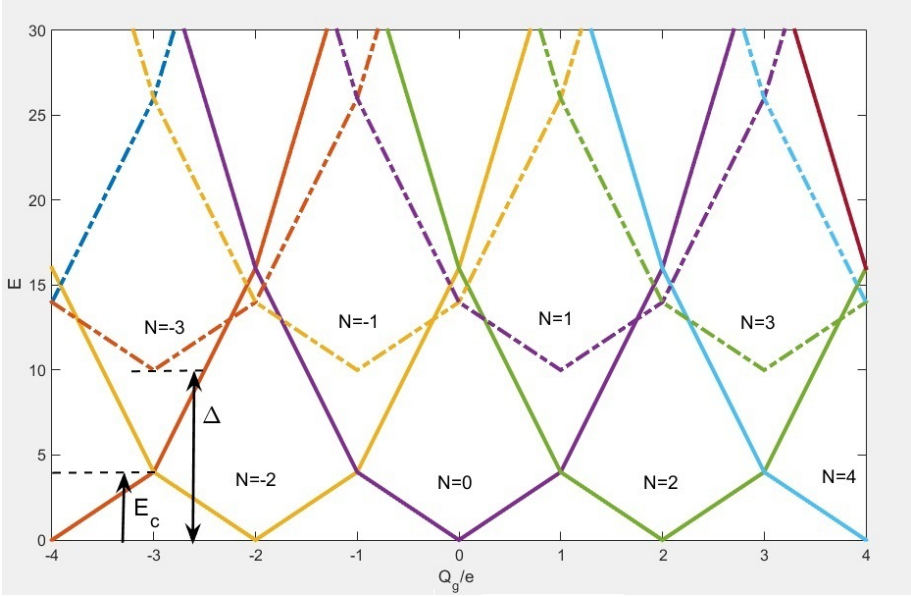

(a)

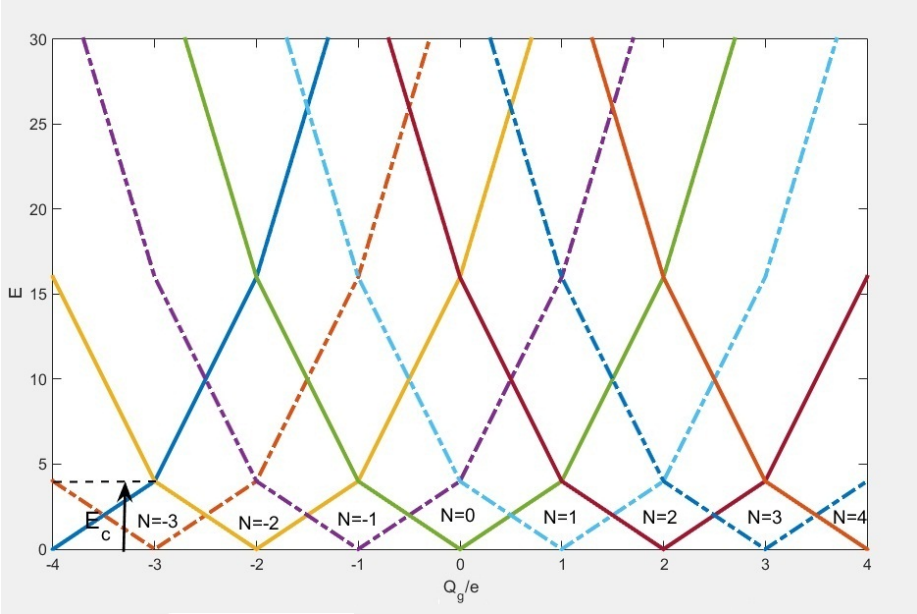

(b)

Figure 5.6: Piecewise linearized energy spectrum of a superconductor having charging energy E_c with varying gate charge Q_g/e for different N, (a) is a conventional superconductor (cf. Figure 5.2 (b)) with the odd states (dashed lines) separated from even states by a gap Δ. (b) A topological superconductor with a pair of zero-energy Majorana fermions (cf. Figure 5.4 (b)).

Chapter 6

Conclusion

In the past, the two-channel Kondo model had been conveniently expressed in terms of Majorana fermion representation by way of the algebra they follow, only because of its mathematical simplicity as explained in Chapter 3. The converse mapping was not considered as the Majorana fermions of such Kondo models did not carry any physical significance beyond their mathematical usage. However, the advent of topological superconductors and the possible appearance of Majorana fermions in condensed matter systems have made this an interesting line of research. Now a novel Kondo effect has been proposed through Majorana bound states appearing at the ends of a p-wave superconductor owing to similar algebraic relations. The topological protection of these Majorana bound states extended to the Kondo effect makes it robust against perturbations. Therefore, a topological Kondo effect may be achieved by the topological degeneracy of Majorana fermions.

The topological Kondo effect, being of multichannel type, leads to a non-Fermi liquid behaviour that is also robust against perturbations and is not prone to disorder. The enhanced conductance of the mesoscopic device acts as a signature of the topological Kondo effect. The Kondo effect can be easily switched off by decoupling one of the leads or by changing the gate charge such that the Kondo effect is not favoured by the effective charging energy. Another clear signature of the topological Kondo effect is given by the local density of states (LDOS) of the lead electrons close to the island which can be directly measured by a scanning tunneling microscope (STM) [96]. Thus this simple realization of the topological Kondo effect does not require fine tuning of parameters, making it experimentally feasible with available technologies. Further studies of the model can be made by coupling the superconducting island to ferromagnetic leads [97]. By changing the charging energy and in turn the Kondo coupling, the transition a ferromagnetic Kondo effect can also be investigated [98].

In conclusion, the topological Kondo effect breaks new ground for the study of non-Fermi liquid physics. It also demonstrates the non-local nature of Majorana fermions which is fundamental to the implementation of fault-tolerant quantum computation systems.

Appendices

Appendix A

Unpaired Majorana fermions in Kitaev's 1D Toy model

The 1D spinless p-wave superconducting chain is described in the second quantization language by the Hamiltonian as

$$H = -t\sum_{j=0}^{N-1}(c_j^\dagger c_{j+1} + c_{j+1}^\dagger c_j) - \sum_{j=0}^{N-1}(\Delta^* c_j^\dagger c_{j+1}^\dagger + \Delta c_{j+1} c_j) - \mu\sum_{j=0}^{N} c_j^\dagger c_j \quad \text{(A.1)}$$

Where c_j and $c_j^\dagger$ are the fermionic operators, i.e. the electron annihilation and creation operator respectively, μ is the chemical potential associated with the number operator $c_j^\dagger c_j = n_j$, t is the hopping amplitude between neighbouring sites in the chain and is the same for all sites throughout the chain. The superconducting gap due to p-wave pairing Δ can be written as $\Delta = |\Delta|e^{i\phi}$, where ϕ is the superconducting phase (here p-wave superconducting pairing phase) and $e^{i\phi}$ is absorbed into the Majorana fermion operators as we define the fermionic operators below,

$$\begin{aligned} c_j &= e^{-i\phi/2}(\gamma_{1,j} + i\gamma_{2,j})/\sqrt{2}, \\ c_j^\dagger &= e^{i\phi/2}(\gamma_{1,j} - i\gamma_{2,j})/\sqrt{2}. \end{aligned} \quad \text{(A.2)}$$

From above, it is evident that Majorana fermions can be obtained by splitting the fermions into real and imaginary parts. Hence,

$$\begin{aligned} \gamma_{1,j} &= (e^{-i\phi/2}c_j^\dagger + e^{i\phi/2}c_j)/\sqrt{2}, \\ \gamma_{2,j} &= i(e^{-i\phi/2}c_j^\dagger - e^{i\phi/2}c_j)/\sqrt{2}. \end{aligned} \quad \text{(A.3)}$$

Thus $\gamma_{i,j}$ is the Majorana operator residing at site j. As two Majorana fermions are required for constructing a fermion, $i = (1, 2)$ indicates the two

Majoranas (at 1 and 2) combining to form a fermion at site j. Clearly the above operators are hermitian and obey the Majorana fermionic relations

$$\begin{aligned} \gamma_{\alpha,i} &= \gamma_{\alpha,i}^{\dagger}, \\ \{\gamma_{\alpha,i}, \gamma_{\beta,j}\} &= \delta_{ij}\delta_{\alpha\beta}. \\ \text{where, } \delta_{xy} &= \begin{cases} 0 & \text{when } x \neq y \\ 1 & \text{when } x = y \end{cases} \end{aligned} \tag{A.4}$$

It can be seen that the fermionic operators are defined similar to $c_j = (\gamma_{1,j} + i\gamma_{2,j})/\sqrt{2}$ except for an additional phase ϕ. Now the Hamiltonian A.1 is simplified to,

$$H = -t\sum_{j=0}^{N-1}(c_j^{\dagger}c_{j+1} + c_{j+1}^{\dagger}c_j) - |\Delta|\sum_{j=0}^{N-1}(c_j^{\dagger}c_{j+1}^{\dagger} + c_{j+1}c_j) - \mu\sum_{j=0}^{N} c_j^{\dagger}c_j \tag{A.5}$$

Now the terms in Kitaev Hamiltonian in terms of Majorana operators become

$$\begin{aligned} c_j^{\dagger}c_{j+1} + c_{j+1}^{\dagger}c_j &= \frac{1}{2}(\gamma_{1,j} - i\gamma_{2,j})(\gamma_{1,j+1} + i\gamma_{2,j+1}) + \frac{1}{2}(\gamma_{1,j+1} - i\gamma_{2,j+1}) \\ &\qquad (\gamma_{1,j} + i\gamma_{2,j}) \\ &= \frac{1}{2}[(\gamma_{1,j}\gamma_{1,j+1} + i\gamma_{1,j}\gamma_{2,j+1} - i\gamma_{2,j}\gamma_{1,j+1} + \gamma_{2,j}\gamma_{2,j+1}) + (\gamma_{1,j+1}\gamma_{1,j} + i\gamma_{1,j+1}\gamma_{2,j} \\ &\qquad - i\gamma_{2,j+1}\gamma_{1,j} + \gamma_{2,j+1}\gamma_{2,j})] \\ &= \frac{1}{2}[\gamma_{1,j}\gamma_{1,j+1} + \gamma_{1,j+1}\gamma_{1,j} + \gamma_{2,j}\gamma_{2,j+1} + \gamma_{2,j+1}\gamma_{2,j} - i\gamma_{2,j+1}\gamma_{1,j} + \\ &\qquad i\gamma_{1,j}\gamma_{2,j+1} - i\gamma_{2,j}\gamma_{1,j+1} + i\gamma_{1,j+1}\gamma_{2,j}] \\ &= \frac{1}{2}[\{\gamma_{1,j}, \gamma_{1,j+1}\} + \{\gamma_{2,j}, \gamma_{2,j+1}\} - i\gamma_{2,j+1}\gamma_{1,j} + i(-\gamma_{2,j+1}\gamma_{1,j}) - \\ &\qquad i(-\gamma_{1,j+1}\gamma_{2,j}) + i\gamma_{1,j+1}\gamma_{2,j}] \\ &= \frac{1}{2}[0 + 0 + 2i\gamma_{1,j+1}\gamma_{2,j} - 2i\gamma_{2,j+1}\gamma_{1,j}]. \end{aligned}$$

The expression is reduced to

$$c_j^{\dagger}c_{j+1} + c_{j+1}^{\dagger}c_j = i[\gamma_{1,j+1}\gamma_{2,j} - \gamma_{2,j+1}\gamma_{1,j}]. \tag{A.6}$$

Now the next part,

$$c_j^\dagger c_{j+1}^\dagger + c_{j+1}c_j = \frac{1}{2}(\gamma_{1,j} - i\gamma_{2,j})(\gamma_{1,j+1} - i\gamma_{2,j+1}) + \frac{1}{2}(\gamma_{1,j+1} + i\gamma_{2,j+1})(\gamma_{1,j} + i\gamma_{2,j})$$

$$= \frac{1}{2}[(\gamma_{1,j}\gamma_{1,j+1} - i\gamma_{1,j}\gamma_{2,j+1} - i\gamma_{2,j}\gamma_{1,j+1} - \gamma_{2,j}\gamma_{2,j+1}) + (\gamma_{1,j+1}\gamma_{1,j} + i\gamma_{1,j+1}\gamma_{2,j} + i\gamma_{2,j+1}\gamma_{1,j} - \gamma_{2,j+1}\gamma_{2,j})]$$

$$= \frac{1}{2}[\gamma_{1,j}\gamma_{1,j+1} + \gamma_{1,j+1}\gamma_{1,j} - \gamma_{2,j}\gamma_{2,j+1} - \gamma_{2,j+1}\gamma_{2,j} + i\gamma_{2,j+1}\gamma_{1,j} - i\gamma_{1,j}\gamma_{2,j+1} - i\gamma_{2,j}\gamma_{1,j+1} + i\gamma_{1,j+1}\gamma_{2,j}]$$

$$= \frac{1}{2}[\{\gamma_{1,j}, \gamma_{1,j+1}\} - \{\gamma_{2,j}, \gamma_{2,j+1}\} + i\gamma_{2,j+1}\gamma_{1,j} - i(-\gamma_{2,j+1}\gamma_{1,j}) - i(-\gamma_{1,j+1}\gamma_{2,j}) + i\gamma_{1,j+1}\gamma_{2,j}]$$

$$= \frac{1}{2}[0 - 0 + 2i\gamma_{2,j+1}\gamma_{1,j} + 2i\gamma_{1,j+1}\gamma_{2,j}].$$

Therefore the expression becomes

$$c_j^\dagger c_{j+1}^\dagger + c_{j+1}c_j = i[\gamma_{2,j+1}\gamma_{1,j} + \gamma_{1,j+1}\gamma_{2,j}]. \tag{A.7}$$

Now moving on to the third term

$$c_j^\dagger c_j = (\frac{\gamma_{1,j} - i\gamma_{2,j}}{\sqrt{2}})(\frac{\gamma_{1,j} + i\gamma_{2,j}}{\sqrt{2}}) = \frac{1}{2}(\gamma_{1,j}\gamma_{1,j} + i\gamma_{1,j}\gamma_{2,j} - i\gamma_{2,j}\gamma_{1,j} + \gamma_{2,j}\gamma_{2,j})$$

Since,

$$\{\gamma_{1,j}, \gamma_{1,j}\} = \gamma_{1,j}\gamma_{1,j} + \gamma_{1,j}\gamma_{1,j} = 1,$$
$$\{\gamma_{1,j}, \gamma_{2,j}\} = \gamma_{1,j}\gamma_{2,j} + \gamma_{2,j}\gamma_{1,j} = 0,$$

$$c_j^\dagger c_j = \frac{1}{2}(\frac{1}{2} + i\gamma_{1,j}\gamma_{2,j} - i(-\gamma_{1,j}\gamma_{2,j}) + \frac{1}{2}) = \frac{1}{2}(1 + 2i\gamma_{1,j}\gamma_{2,j}) = \frac{1}{2} + i\gamma_{1,j}\gamma_{2,j}$$

Therefore,

$$\begin{aligned} c_j^\dagger c_j &= \frac{1}{2} + i\gamma_{1,j}\gamma_{2,j} \\ &\text{or} \\ &= \frac{1}{2} - i\gamma_{2,j}\gamma_{1,j}. \end{aligned} \tag{A.8}$$

Now the Kitaev chain in terms of Majorana is obtained by substituting (A.6),(A.7) and (A.8) in the Hamiltonian (A.5)

$$H = -t\sum_{j=0}^{N-1}(i[\gamma_{1,j+1}\gamma_{2,j} - \gamma_{2,j+1}\gamma_{1,j}]) - |\Delta|\sum_{j=0}^{N-1}(i[\gamma_{2,j+1}\gamma_{1,j} + \gamma_{1,j+1}\gamma_{2,j}]) - \mu\sum_{i=0}^{N}(\frac{1}{2} + i\gamma_{1,j}\gamma_{2,j}),$$

$$H = \sum_{j=0}^{N-1}(i(-t-|\Delta|)\gamma_{1,j+1}\gamma_{2,j} + i(t-|\Delta|)\gamma_{2,j+1}\gamma_{1,j}). - \mu\sum_{j=0}^{N}(\frac{1}{2} + i\gamma_{1,j}\gamma_{2,j})$$

Therefore, the Hamiltonian in terms of Majorana operators is given by

$$H = i\sum_{j=0}^{N-1}((t-|\Delta|)\gamma_{2,j+1}\gamma_{1,j} - (t+|\Delta|)\gamma_{1,j+1}\gamma_{2,j}) - \mu\sum_{j=0}^{N}(\frac{1}{2} + i\gamma_{1,j}\gamma_{2,j}). \tag{A.9}$$

For the case of $\mu = 0$ and $t = |\Delta|$, (A.9) reduces to

$$H = -2it\sum_{j=0}^{N-1}(\gamma_{1,j+1}\gamma_{2,j}). \tag{A.10}$$

Now define new set of fermionic operators such that,

$$\begin{aligned} d_i &= (\gamma_{2,j} + i\gamma_{1,j+1})/\sqrt{2} \\ , d_i^\dagger &= (\gamma_{2,j} - i\gamma_{1,j+1})/\sqrt{2}. \end{aligned} \tag{A.11}$$

Then

$$d_i^\dagger d_i = \frac{1}{2} - i\gamma_{1,j+1}\gamma_{2,j}$$

Hence (A.10) becomes

$$H = 2t \sum_{j=0}^{N-1} (d_i^\dagger d_i - \frac{1}{2}). \tag{A.12}$$

The unpaired Majorana fermions absent from the above Hamiltonian are identified in Section 4.4 and combined to form a non-local fermion.

Appendix B

Effective tunneling Hamiltonian involving Majorana fermions

Electrons hopping into the superconducting wires a and b shown in Figure 4.1 are represented by electron operators in terms of the Majorana fermion operators associated with the Majorana bound state at the end of the wires. In wire a,

$$\begin{aligned} \psi_a^\dagger &= e^{i\phi/2}\left[\xi_0^*(x)\gamma_0^\dagger + \xi_1^*(x)\gamma_1^\dagger\right], \\ \psi_a &= e^{-i\phi/2}\left[\xi_0(x)\gamma_0 + \xi_1(x)\gamma_1\right], \end{aligned} \tag{B.1}$$

where $\gamma_1(\gamma_0)$ denotes the Majorana bound state at the end of wire a coupled to lead 1 (not lead). While in wire b,

$$\begin{aligned} \psi_b^\dagger &= e^{i\phi/2}\left[\xi_2^*(x)\gamma_2^\dagger + \xi_3^*(x)\gamma_3^\dagger\right], \\ \psi_b &= e^{-i\phi/2}\left[\xi_2(x)\gamma_2 + \xi_3(x)\gamma_3\right], \end{aligned} \tag{B.2}$$

where $\gamma_2(\gamma_3)$ denotes the Majorana bound state at the end of wire b coupled to lead 2 (lead 3). If t_j is the tunneling probability of an electron tunneling from lead j into a superconducting wire, then the tunneling processes at the contact between lead 1 and wire a can be expressed as

$$\begin{aligned} \text{Lead 1} \rightarrow \text{Wire } a &= t_1\psi_a^\dagger\psi_1 = t_1 e^{i\phi/2}\xi_1^*(R_1)\gamma_1^\dagger\psi_1, \\ \text{Wire } a \rightarrow \text{Lead 1} &= t_1\psi_1^\dagger\psi_a = \psi_1^\dagger t_1 e^{-i\phi/2}\xi_1(R_1)\gamma_1, \end{aligned} \tag{B.3}$$

where R_1 is the coordinate of the contact (at which the Majorana wave function ξ_1 is also peaked). In general, for an electron hopping between a lead and a superconductor, electron tunneling is given by

$$\begin{aligned} \text{Lead j} \rightarrow \text{Wire} &= t_j e^{i\phi/2}\xi_j^*(R_j)\gamma_j^\dagger\psi_j, \\ \text{Wire} \rightarrow \text{Lead j} &= \psi_j^\dagger t_j e^{-i\phi/2}\xi_j(R_j)\gamma_j. \end{aligned} \tag{B.4}$$

B.1 Transition rates

In order to obtain the effective lead-lead tunneling Hamiltonian one needs to consider the probability of electrons tunneling from one lead to another. This is accomplished by employing the formula for second-order transition of states, based on time-dependent perturbation theory [99],

$$T^{(2)}_{j\to k} = \sum_{l\neq j} \frac{\langle k|H_T|l\rangle\langle l|H_T|j\rangle}{(E_j - E_l)} \tag{B.5}$$

where, for notational simplicity, we have absorbed a factor of $\hbar/2\pi$ into the definition of the transition rate $T^{(2)}_{j\to k}$. The tunneling of an electron from lead j to lead k, involves two different intermediate states. Let us look at these intermediate processes in detail.

Case A

The first case involves a two step process, with (i) an electron in lead j at the Fermi level tunneling into the superconducting island, occupying the first available energy level on the island and next, (ii) the tunneling from the island into the lead k.

Step 1: Lead → Island

Tunneling from the lead into the superconducting island $\langle l|H_T|j\rangle$ is described using the states,

$|j\rangle = |\text{Electron in lead j}\rangle \otimes |\text{Initial } N \text{ electrons on the island}\rangle$, along with
$|l\rangle = |\text{Electron in the first available level on the island}\rangle \otimes$
$|N \text{ electrons on the island}\rangle$.

Here $N = 2n$, where n is the number of Cooper pairs on the island. The energy of the initial state $|j\rangle$ is the sum of the energy of an electron at the Fermi level in the lead, and the charging energy $E_0(N)$ of N electrons on the island (cf. (5.2). Energy in the initial state is $E^A_j = \varepsilon_{\vec{k}} + E_0(N)$. With the same reasoning, the energy of the intermediate state, $E^A_l = E_0(N+1)$.

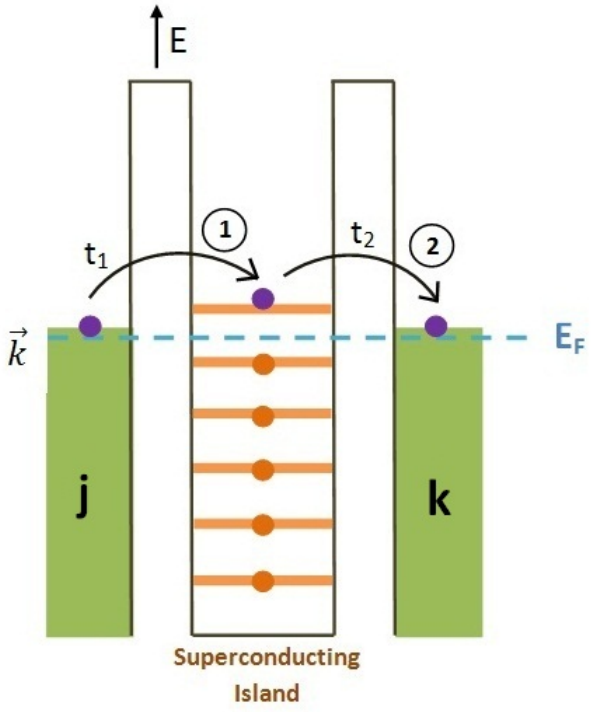

Figure B.1: Tunneling of electron from lead 'j' to lead 'k' via superconducting island.

Step 2: Island → Lead

The tunneling from the superconducting island to the lead, $\langle k|H_T|l\rangle$, is expressed using the states,

$$|l\rangle = |\text{Electron in the first available level on the island}\rangle \otimes |N \text{ electrons on the island}\rangle\,,$$

$$|k\rangle = |\text{Electron in the other lead }\rangle \otimes |\text{Initial } N \text{ electrons on the island}\rangle\,.$$

Since the transition is independent of the energy of the final state, we compute from B.5,

$$T^{(2)}_{j\to k}(A) = \sum_{l\neq j} \frac{\langle k|H_T|l\rangle\langle l|H_T|j\rangle}{\varepsilon_{\vec{k}} + E_0(N) - E_0(N+1)}. \tag{B.6}$$

Because an electron in a lead is at the Fermi level, we can put $\epsilon_{\vec{k}} \approx \epsilon_F$, and write,

$$T^{(2)}_{j\to k}(A) \approx \sum_{l\neq j} \frac{\langle k|H_T|l\rangle\langle l|H_T|j\rangle}{\varepsilon_F + E_0(N) - E_0(N+1)}. \tag{B.7}$$

Choosing an energy scale such that $\varepsilon_F = 0$, we obtain

$$T^{(2)}_{j\to k}(A) = \sum_{l\neq j} \frac{\langle k|H_T|l\rangle\langle l|H_T|j\rangle}{E_0(N) - E_0(N+1)}. \tag{B.8}$$

Case: B

The second case involves an electron on the superconducting island first hopping to to one of the leads. This creates an empty level on the island, allowing an electron in the other lead to jump into the island, making the number of electrons on the superconducting island the same as that in the initial state. The energy of the initial state is given by $E^B_j = E_0(N) + \varepsilon_{\vec{k}}$.

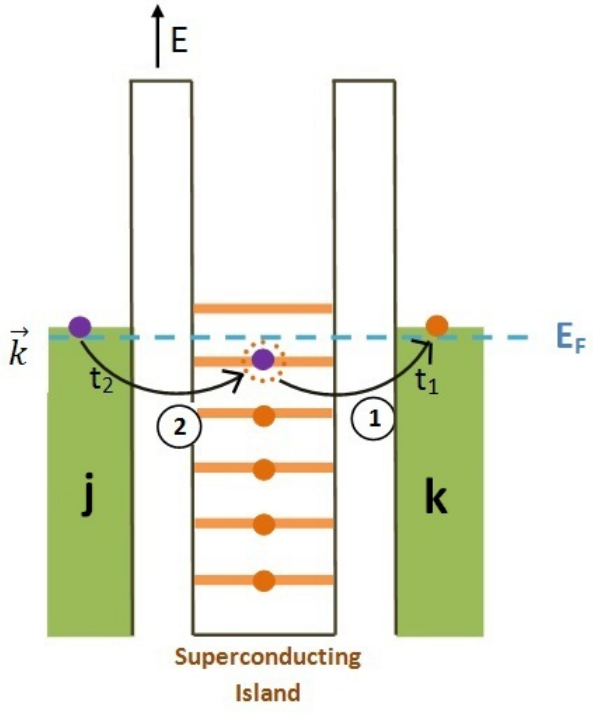

Figure B.2: Tunneling of electron from superconducting island to lead 'k' and from lead 'j' to island.

Now the energy of the intermediate state is the charging energy of $N-1$ electrons on the island plus the kinetic energies of TWO electrons in the leads. Therefore, The energy of the intermediate state $= E^B_l = E_0(N-1) + 2\epsilon_{\vec{k}}$

An expression for the transition is obtained similar to the first case as

$$T^{(2)}_{j\to k}(B) = \sum_{l\neq j} \frac{\langle k|H_T|l\rangle\langle l|H_T|j\rangle}{E_0(N) + \varepsilon_{\vec{k}} - E_0(N-1)}. \tag{B.9}$$

Again putting $\epsilon_{\vec{k}} \approx \epsilon_F = 0$,

$$T^{(2)}_{j\to k}(B) = \sum_{l\neq j} \frac{\langle k|H_T|l\rangle\langle l|H_T|j\rangle}{E_0(N) - E_0(N-1)}. \tag{B.10}$$

B.2 Tunneling of electrons between leads

Now using the tunneling probabilities computed above in B.4 and transition probabilities in B.8 and B.10, the tunneling of a single electron between the leads in the topological superconductor set-up is obtained in the following way.

Consider first tunneling of an electron from lead 2 to lead 3, illustrated in Figure 4.1. It involves two intermediate processes with one involving the electron tunneling from lead 2 to wire b first, and from wire b towards lead 3, $T^{(2)}_{2\to 3}(A)$. The other process involves first, tunneling from wire b to lead 3 and next, into wire b from lead 2, $T^{(2)}_{2\to 3}(B)$.

$$\begin{aligned} T^{(2)}_{2\to 3}(A) &= \frac{\langle 3|H_T|b\rangle\langle b|H_T|2\rangle}{(E_2 - E_b)} \\ &= \frac{\psi_3^\dagger t_3 e^{-i\phi/2}\xi_3(R_3)\gamma_3 t_2 e^{i\phi/2}\xi_2^*(R_2)\gamma_2^\dagger\psi_2}{E_0(N) - E_0(N+1)}. \end{aligned}$$

Note $\xi_i(R_j) = \delta_{ij}$ since Majorana modes localized at the ends of a wire are assumed to have zero wave function overlap. Having thus neglected the broadening of the localized wave function, we obtain

$$T^{(2)}_{2\to 3}(A) = \frac{t_2 t_3 \psi_3^\dagger \gamma_3 \gamma_2^\dagger \psi_2}{E_0(N) - E_0(N+1)}. \tag{B.11}$$

Similarly,

$$\begin{aligned} T^{(2)}_{2\to 3}(B) &= \frac{\langle b|H_T|2\rangle\langle 3|H_T|b\rangle}{(E_b - E_3)} \\ &= \frac{\gamma_3 t_2 e^{i\phi/2}\xi_2^*(R_2)\gamma_2^\dagger\psi_2\psi_3^\dagger t_3 e^{-i\phi/2}\xi_3(R_3)}{E_0(N) - E_0(N-1)} \end{aligned}$$

$$T^2_{2\to 3}(B) = \frac{t_2 t_3 \gamma_2^\dagger \psi_2 \psi_3^\dagger \gamma_3}{E_0(N) - E_0(N-1)}. \tag{B.12}$$

The sum of these two intermediate processes gives the process of electron tunneling from lead 2 to lead 3,

$$\begin{aligned} T^{(2)}_{2\to 3} &= T^{(2)}_{2\to 3}(A) + T^{(2)}_{2\to 3}(B) \\ &= \frac{t_2 t_3 \psi_3^\dagger \gamma_3 \gamma_2^\dagger \psi_2}{E_0(N) - E_0(N+1)} + \frac{t_2 t_3 \gamma_2^\dagger \psi_2 \psi_3^\dagger \gamma_3}{E_0(N) - E_0(N-1)} \\ &= \frac{t_2 t_3 \psi_3^\dagger \gamma_3 \gamma_2 \psi_2}{E_0(N) - E_0(N+1)} + \frac{t_2 t_3 \gamma_2 \psi_2 \psi_3^\dagger \gamma_3}{E_0(N) - E_0(N-1)}, \end{aligned}$$

where we have used $\gamma = \gamma^\dagger$ in the second line. We can also use the fermionic anticommutation rules to simplify this further:

$$\begin{aligned} \gamma_3 \gamma_2 &= -\gamma_2 \gamma_3 \\ \psi_2 \psi_3^\dagger &= -\psi_3^\dagger \psi_2, \end{aligned}$$

$$\begin{aligned} T^{(2)}_{2\to 3} &= \frac{t_2 t_3 (-\gamma_2 \gamma_3) \psi_3^\dagger \psi_2}{E_0(N) - E_0(N+1)} + \frac{t_2 t_3 \gamma_2 \gamma_3 (-\psi_3^\dagger \psi_2)}{E_0(N) - E_0(N-1)} \\ &= t_2 t_3 \gamma_2 \gamma_3 \psi_3^\dagger \psi_2 \left\{ \frac{-1}{E_0(N) - E_0(N+1)} + \frac{-1}{E_0(N) - E_0(N-1)} \right\} \\ &= t_2 t_3 \gamma_2 \gamma_3 \psi_3^\dagger \psi_2 \left\{ \frac{1}{U_+} + \frac{1}{U_-} \right\}. \end{aligned} \tag{B.13}$$

where $U_\pm = E_0(N \pm 1) - E_0(N)$. Generalizing, we get the effective tunneling between different leads as

$$T^{(2)}_{i\to j} = \sum_{i \neq j} t_i t_j \gamma_i \gamma_j \psi_j^\dagger \psi_i \left\{ \frac{1}{U_+} + \frac{1}{U_-} \right\}. \tag{B.14}$$

For the case of $i = j$, let us consider the tunneling at lead 1 which involves tunneling of an electron from lead 1 into wire a and tunneling back to lead 1 from wire a. An expression similar to the one above is obtained,

$$T^{(2)}_{1\to 1} = \frac{t_1^2 \psi_1^\dagger \gamma_1 \gamma_1^\dagger \psi_1}{E_0(N) - E_0(N+1)} + \frac{t_1^2 \gamma_1^\dagger \psi_1 \psi_1^\dagger \gamma_1}{E_0(N) - E_0(N-1)}.$$

Since $\gamma = \gamma^\dagger$ and $\gamma^2 = 1$,

$$T^2_{1\to 1} = \frac{t_1^2 \psi_1^\dagger \psi_1}{E_0(N) - E_0(N+1)} + \frac{t_1^2 \psi_1 \psi_1^\dagger}{E_0(N) - E_0(N-1)}.$$

Revoking the fermionic anti-commutation properties with $\psi_1^\dagger\psi_1 + \psi_1\psi_1^\dagger = 1$, the above expression becomes

$$\begin{aligned} T^{(2)}_{1\to 1} &= \frac{t_1^2\psi_1^\dagger\psi_1}{E_0(N) - E_0(N+1)} + \frac{t_1^2(1-\psi_1^\dagger\psi_1)}{E_0(N) - E_0(N-1)} \\ &= t_1^2\psi_1^\dagger\psi_1\left\{\frac{1}{E_0(N) - E_0(N+1)} + \frac{-1}{E_0(N) - E_0(N-1)}\right\} + \\ &\qquad\qquad \frac{t_1^2}{E_0(N) - E_0(N-1)} \end{aligned} \tag{B.15}$$

It can be rewritten as

$$\begin{aligned} T^{(2)}_{1\to 1} &= -t_1^2\psi_1^\dagger\psi_1\left\{\frac{1}{E_0(N+1) - E_0(N)} + \frac{-1}{E_0(N-1) - E_0(N)}\right\} + const. \\ &= -t_1^2\psi_1^\dagger\psi_1\left\{\frac{1}{U_+} - \frac{1}{U_-}\right\} + const. \end{aligned} \tag{B.16}$$

In general,

$$T^{(2)}_{j\to j} = -t_j^2\psi_j^\dagger\psi_j\left\{\frac{1}{U_+} - \frac{1}{U_-}\right\} + const. \tag{B.17}$$

The effective tunneling Hamiltonian H_T is thus given by

$$H_T = \sum_{i\neq j} t_i t_j \gamma_i^\dagger\gamma_j\psi_j^\dagger\psi_i\left\{\frac{1}{U_+} + \frac{1}{U_-}\right\} - \sum_j t_j^2\psi_j^\dagger\psi_j\left\{\frac{1}{U_+} - \frac{1}{U_-}\right\} + const. \tag{B.18}$$

Introducing the constants $\lambda_{ij}^{\pm} = t_i t_j\left(\frac{1}{U_+} \pm \frac{1}{U_-}\right)$,

$$H_T = \sum_{i\neq j}\lambda_{ij}^+\gamma_i^\dagger\gamma_j\psi_j^\dagger\psi_i - \sum_j \lambda_{jj}^-\psi_j^\dagger\psi_j. \tag{B.19}$$

To conclude, the effective Hamiltonian of the system, $H_{\text{eff}} = H_{\text{leads}} + H_T$ can be written as,

$$H_{\text{eff}} = H_{\text{leads}} + \sum_{i\neq j}\lambda_{ij}^+\gamma_i^\dagger\gamma_j\psi_j^\dagger\psi_i - \sum_j \lambda_{jj}^-\psi_j^\dagger\psi_j \tag{B.20}$$

from which the Kondo Hamiltonian can be extracted as discussed in Section 5.3.

Bibliography

[1] B. Béri and N. R. Cooper, "Topological Kondo effect with Majorana fermions," *Physical Review letters*, vol. 109, no. 15, p. 156803, 2012.

[2] D. Ter Haar, *Collected papers of LD Landau*. Elsevier, 2013.

[3] L. D. Landau and E. M. Lifshitz, *Course of theoretical physics*. Elsevier, 2013.

[4] S. Todadri, "Quantum matters: Physics beyond landau's paradigms," *International Journal of Modern Physics B*, vol. 20, no. 19, pp. 2603–2611, 2006.

[5] S. Todadri, L. Balents, S. Sachdev, A. Vishwanath, and M. P. Fisher, "Quantum criticality beyond the landau-ginzburg-wilson paradigm," *Physical Review B*, vol. 70, no. 14, p. 144407, 2004.

[6] P. W. Anderson, *Basic notions of condensed matter physics*. No. v. 55 in Frontiers in Physics, Benjamin/Cummings Pub. Co., Advanced Book Program, 1984.

[7] A. J. Schofield, "Non-fermi liquids," *Contemporary Physics*, vol. 40, no. 2, pp. 95–115, 1999.

[8] A. Damascelli, Z. Hussain, and Z.-X. Shen, "Angle-resolved photoemission studies of the cuprate superconductors," *Reviews of modern physics*, vol. 75, no. 2, p. 473, 2003.

[9] P. W. Anderson *et al.*, *The theory of superconductivity in the high-Tc cuprate superconductors*, vol. 446. Princeton University Press Princeton, NJ, 1997.

[10] G. Stewart, "Heavy-fermion systems," *Reviews of Modern Physics*, vol. 56, no. 4, p. 755, 1984.

[11] P. Coleman, "Theories of non-fermi liquid behavior in heavy fermions," *Physica B: Condensed Matter*, vol. 259, pp. 353–358, 1999.

[12] D. C. Tsui, H. L. Stormer, and A. C. Gossard, "Two-dimensional magnetotransport in the extreme quantum limit," *Physical Review Letters*, vol. 48, no. 22, p. 1559, 1982.

[13] E. Eriksson, *Correlations in low-dimensional quantum many-particle systems*. PhD thesis, Göteborgs universitet, 2013.

[14] T. Giamarchi, "Quantum physics in one dimension," 2004.

[15] S. Sachdev, *Quantum phase transitions*. Wiley Online Library, 2007.

[16] A. C. Hewson, *The Kondo problem to heavy fermions*, vol. 2. Cambridge university press, 1997.

[17] M. Greiter, "Is electromagnetic gauge invariance spontaneously violated in superconductors?," *Annals of Physics*, vol. 319, no. 1, pp. 217–249, 2005.

[18] X.-G. Wen, "Topological orders and edge excitations in fractional quantum Hall states," *Advances in Physics*, vol. 44, no. 5, pp. 405–473, 1995.

[19] X.-G. Wen and Q. Niu, "Ground-state degeneracy of the fractional quantum Hall states in the presence of a random potential and on high-genus riemann surfaces," *Physical Review B*, vol. 41, no. 13, p. 9377, 1990.

[20] V. Rajan, J. H. Lowenstein, and N. Andrei, "Thermodynamics of the Kondo model," *Physical Review Letters*, vol. 49, no. 7, p. 497, 1982.

[21] M. Grobis, I. G. Rau, R. M. Potok, and D. Goldhaber-Gordon, "The Kondo effect in mesoscopic quantum dots," *Handbook of Magnetism and Advanced Magnetic Materials*, 2007.

[22] A. Y. Kitaev, "Unpaired Majorana fermions in quantum wires," *Physics-Uspekhi*, vol. 44, no. 10S, p. 131, 2001.

[23] J. Alicea, "New directions in the pursuit of Majorana fermions in solid state systems," *Reports on Progress in Physics*, vol. 75, no. 7, p. 076501, 2012.

[24] A. Y. Kitaev, "Fault-tolerant quantum computation by anyons," *Annals of Physics*, vol. 303, no. 1, pp. 2–30, 2003.

[25] W. De Haas, J. De Boer, and G. Van den Berg, "The electrical resistance of gold, copper and lead at low temperatures," *Physica*, vol. 1, no. 7, pp. 1115–1124, 1934.

[26] G. Van den Berg, "Anomalies in dilute metallic solutions of transition elements," *Progress in Low Temperature Physics (Netherlands)*, vol. 4, 1964.

[27] J. Kondo, "Resistance minimum in dilute magnetic alloys," *Progress of theoretical physics*, vol. 32, no. 1, pp. 37–49, 1964.

[28] P. W. Anderson, "A poor man's derivation of scaling laws for the Kondo problem," *Journal of Physics C: Solid State Physics*, vol. 3, no. 12, p. 2436, 1970.

[29] K. G. Wilson, "The renormalization group: Critical phenomena and the Kondo problem," *Reviews of Modern Physics*, vol. 47, no. 4, p. 773, 1975.

[30] E. Pavarini, P. Coleman, and E. Koch, "Many-body physics: From Kondo to Hubbard," tech. rep., Theoretische Nanoelektronik, 2015.

[31] P. Nozieres and A. Blandin, "Kondo effect in real metals," *Journal de Physique*, vol. 41, no. 3, pp. 193–211, 1980.

[32] B. A. Jones, *The Kondo effect*. John Wiley & Sons Ltd, 2007.

[33] N. Andrei and C. Destri, "Solution of the multichannel Kondo problem," *Physical Review letters*, vol. 52, no. 5, p. 364, 1984.

[34] I. Affleck and A. W. Ludwig, "The Kondo effect, conformal field theory and fusion rules," *Nuclear Physics B*, vol. 352, no. 3, pp. 849–862, 1991.

[35] V. J. Emery and S. Kivelson, "Mapping of the two-channel Kondo problem to a resonant-level model," *Physical Review B*, vol. 46, no. 17, p. 10812, 1992.

[36] G. Toulouse, "Infinite-u Anderson hamiltonian for dilute alloys," *Physical Review B*, vol. 2, no. 2, p. 270, 1970.

[37] P. Coleman, L. Ioffe, and A. Tsvelik, "Pedestrian approach to the two-channel Kondo model," *arXiv preprint cond-mat/9504006*, 1995.

[38] G.-M. Zhang, A. C. Hewson, and R. Bulla, "Majorana fermion formulation of the two channel Kondo model," *Solid state communications*, vol. 112, no. 2, pp. 105–108, 1999.

[39] I. Affleck and A. W. Ludwig, "Critical theory of overscreened Kondo fixed points," *Nuclear Physics B*, vol. 360, no. 2, pp. 641–696, 1991.

[40] M. Fabrizio and A. O. Gogolin, "Toulouse limit for the overscreened four-channel Kondo problem," *Physical Review B*, vol. 50, no. 23, p. 17732, 1994.

[41] D. L. Cox and A. Zawadowski, "Exotic Kondo effects in metals: magnetic ions in a crystalline electric field and tunnelling centres," *Advances in Physics*, vol. 47, no. 5, pp. 599–942, 1998.

[42] Y. V. Nazarov and Y. M. Blanter, *Quantum transport: introduction to nanoscience*. Cambridge University Press, 2009.

[43] C. w. Beenakker, "Theory of coulomb-blockade oscillations in the conductance of a quantum dot," *Physical Review B*, vol. 44, no. 4, p. 1646, 1991.

[44] S. M. Cronenwett, T. H. Oosterkamp, and L. P. Kouwenhoven, "A tunable Kondo effect in quantum dots," *Science*, vol. 281, no. 5376, pp. 540–544, 1998.

[45] R. Potok, I. Rau, H. Shtrikman, Y. Oreg, and D. Goldhaber-Gordon, "Observation of the two-channel Kondo effect," *Nature*, vol. 446, no. 7132, pp. 167–171, 2007.

[46] Z. Iftikhar, S. Jezouin, A. Anthore, U. Gennser, F. Parmentier, A. Cavanna, and F. Pierre, "Two-channel Kondo effect and renormalization flow with macroscopic quantum charge states," *Nature*, vol. 526, no. 7572, pp. 233–236, 2015.

[47] A. Keller, L. Peeters, C. Moca, I. Weymann, D. Mahalu, V. Umansky, G. Zaránd, and D. Goldhaber-Gordon, "Universal fermi liquid crossover and quantum criticality in a mesoscopic system," *Nature*, vol. 526, no. 7572, pp. 237–240, 2015.

[48] K. Le Hur, "Condensed-matter physics: Quantum dots and the Kondo effect," *Nature*, vol. 526, no. 7572, pp. 203–204, 2015.

[49] M. Nakahara, *Geometry, topology and physics*. CRC Press, 2003.

[50] M. Z. Hasan and C. L. Kane, "Colloquium: topological insulators," *Reviews of Modern Physics*, vol. 82, no. 4, p. 3045, 2010.

[51] H. A. Kramers, "Théorie générale de la rotation paramagnétique dans les cristaux," *Proc. Acad. Amst*, vol. 33, pp. 959–972, 1930.

[52] X.-L. Qi and S.-C. Zhang, "Topological insulators and superconductors," *Reviews of Modern Physics*, vol. 83, no. 4, p. 1057, 2011.

[53] C. L. Kane and E. J. Mele, "A new spin on the insulating state," *Science*, vol. 314, no. 5806, pp. 1692–1693, 2006.

[54] C. L. Kane and E. J. Mele, "Quantum spin Hall effect in graphene," *Physical Review letters*, vol. 95, no. 22, p. 226801, 2005.

[55] G. E. Volovik, "An analog of the quantum Hall effect in a superfluid 3 he film," 1988.

[56] A. P. Schnyder, S. Ryu, A. Furusaki, and A. W. Ludwig, "Classification of topological insulators and superconductors in three spatial dimensions," *Physical Review B*, vol. 78, no. 19, p. 195125, 2008.

[57] L. Fu and C. L. Kane, "Superconducting proximity effect and Majorana fermions at the surface of a topological insulator," *Physical Review letters*, vol. 100, no. 9, p. 096407, 2008.

[58] N. Read and D. Green, "Paired states of fermions in two dimensions with breaking of parity and time-reversal symmetries and the fractional quantum Hall effect," *Physical Review B*, vol. 61, no. 15, p. 10267, 2000.

[59] D. A. Ivanov, "Non-abelian statistics of half-quantum vortices in p-wave superconductors," *Physical Review letters*, vol. 86, no. 2, p. 268, 2001.

[60] G. E. Volovik, "Fermion zero modes on vortices in chiral superconductors," *JETP Letters*, vol. 70, no. 9, pp. 609–614, 1999.

[61] T. Han and B. Zhang, "Signatures for Majorana neutrinos at hadron colliders," *Physical Review letters*, vol. 97, no. 17, p. 171804, 2006.

[62] F. T. Avignone III, S. R. Elliott, and J. Engel, "Double beta decay, Majorana neutrinos, and neutrino mass," *Reviews of Modern Physics*, vol. 80, no. 2, p. 481, 2008.

[63] M. Leijnse and K. Flensberg, "Introduction to topological superconductivity and Majorana fermions," *Semiconductor Science and Technology*, vol. 27, no. 12, p. 124003, 2012.

[64] S. D. Sarma, C. Nayak, and S. Tewari, "Proposal to stabilize and detect half-quantum vortices in strontium ruthenate thin films: Non-abelian braiding statistics of vortices in a $p_x + ip_y$ superconductor," *Physical Review B*, vol. 73, no. 22, p. 220502, 2006.

[65] G. Moore and N. Read, "Nonabelions in the fractional quantum Hall effect," *Nuclear Physics B*, vol. 360, no. 2, pp. 362–396, 1991.

[66] C. Nayak, S. H. Simon, A. Stern, M. Freedman, and S. D. Sarma, "Non-abelian anyons and topological quantum computation," *Reviews of Modern Physics*, vol. 80, no. 3, p. 1083, 2008.

[67] F. Wilczek, *Fractional statistics and anyon superconductivity*, vol. 5. World Scientific, 1990.

[68] X.-G. Wen, "Gapless boundary excitations in the quantum Hall states and in the chiral spin states," *Physical Review B*, vol. 43, no. 13, p. 11025, 1991.

[69] S. D. Sarma, M. Freedman, and C. Nayak, "Topologically protected qubits from a possible non-abelian fractional quantum Hall state," *Physical Review letters*, vol. 94, no. 16, p. 166802, 2005.

[70] V. Mourik, K. Zuo, S. Frolov, S. Plissard, E. Bakkers, and L. Kouwenhoven, "Signatures of Majorana fermions in hybrid superconductor-semiconductor nanowire devices," *Science*, vol. 336, no. 6084, pp. 1003–1007, 2012.

[71] J. Williams, A. J. Bestwick, P. Gallagher, S. S. Hong, Y. Cui, A. S. Bleich, J. G. Analytis, I. R. Fisher, and D. Goldhaber-Gordon, "Unconventional Josephson effect in hybrid superconductor-topological insulator devices," *Physical Review letters*, vol. 109, no. 5, p. 056803, 2012.

[72] A. Das, Y. Ronen, Y. Most, Y. Oreg, M. Heiblum, and H. Shtrikman, "Zero-bias peaks and splitting in an al-inas nanowire topological superconductor as a signature of Majorana fermions," *Nature Physics*, vol. 8, no. 12, pp. 887–895, 2012.

[73] M. Gong, G. Chen, S. Jia, and C. Zhang, "Searching for Majorana fermions in 2d spin-orbit coupled Fermi superfluids at finite temperature," *Physical Review letters*, vol. 109, no. 10, p. 105302, 2012.

[74] M. Deng, C. Yu, G. Huang, M. Larsson, P. Caroff, and H. Xu, "Anomalous zero-bias conductance peak in a nb–insb nanowire–nb hybrid device," *Nano letters*, vol. 12, no. 12, pp. 6414–6419, 2012.

[75] S. Tewari, S. D. Sarma, C. Nayak, C. Zhang, and P. Zoller, "Quantum computation using vortices and Majorana zero modes of a $p_x + ip_y$ superfluid of fermionic cold atoms," *Physical Review letters*, vol. 98, no. 1, p. 010506, 2007.

[76] V. Gurarie, L. Radzihovsky, and A. Andreev, "Quantum phase transitions across a p-wave feshbach resonance," *Physical Review letters*, vol. 94, no. 23, p. 230403, 2005.

[77] J. Klinovaja, S. Gangadharaiah, and D. Loss, "Electric-field-induced Majorana fermions in armchair carbon nanotubes," *Physical Review letters*, vol. 108, no. 19, p. 196804, 2012.

[78] J. D. Sau and S. Tewari, "Majorana fermions in carbon nanotubes," *arXiv preprint arXiv:1111.5622*, 2011.

[79] R. Egger and K. Flensberg, "Emerging dirac and Majorana fermions for carbon nanotubes with proximity-induced pairing and spiral magnetic field," *Physical Review B*, vol. 85, no. 23, p. 235462, 2012.

[80] P. Hosur, P. Ghaemi, R. S. Mong, and A. Vishwanath, "Majorana modes at the ends of superconductor vortices in doped topological insulators," *Physical Review letters*, vol. 107, no. 9, p. 097001, 2011.

[81] Y. Oreg, G. Refael, and F. von Oppen, "Helical liquids and Majorana bound states in quantum wires," *Physical Review letters*, vol. 105, no. 17, p. 177002, 2010.

[82] Y. E. Kraus, A. Auerbach, H. Fertig, and S. H. Simon, "Majorana fermions of a two-dimensional $p_x + ip_y$ superconductor," *Physical Review B*, vol. 79, no. 13, p. 134515, 2009.

[83] J. D. Sau, R. M. Lutchyn, S. Tewari, and S. D. Sarma, "Generic new platform for topological quantum computation using semiconductor heterostructures," *Physical review letters*, vol. 104, no. 4, p. 040502, 2010.

[84] P. Fulde and R. A. Ferrell, "Superconductivity in a strong spin-exchange field," *Physical Review*, vol. 135, no. 3A, p. A550, 1964.

[85] A. Larkin and Y. Ovchinnikov, "Inhomogeneous state of superconductors (production of superconducting state in ferromagnet with Fermi surfaces, examining Green function)," *Soviet Physics-JETP*, vol. 20, pp. 762–769, 1965.

[86] Y. Nakamura, Y. A. Pashkin, and J. Tsai, "Coherent control of macroscopic quantum states in a single-cooper-pair box," *Nature*, vol. 398, no. 6730, pp. 786–788, 1999.

[87] P. W. Anderson, "Chapter i the Josephson effect and quantum coherence measurements in superconductors and superfluids," vol. 5 of *Progress in Low Temperature Physics*, pp. 1 – 43, Elsevier, 1967.

[88] P. A. Carruthers and M. M. Nieto, "Coherent states and the number-phase uncertainty relation," *Physical Review Letters*, vol. 14, no. 11, p. 387, 1965.

[89] A. M. Zagoskin, *Quantum Engineering: Theory and Design of Quantum Coherent Structures*. Cambridge University Press, 2011.

[90] T. Duty, D. Gunnarsson, K. Bladh, and P. Delsing, "Coherent dynamics of a Josephson charge qubit," *Physical Review B*, vol. 69, no. 14, p. 140503, 2004.

[91] M. Tinkham, *Introduction to superconductivity*. Courier Corporation, 2012.

[92] M. Tuominen, J. Hergenrother, T. Tighe, and M. Tinkham, "Experimental evidence for parity-based 2e periodicity in a superconducting single-electron tunneling transistor," *Physical review letters*, vol. 69, no. 13, p. 1997, 1992.

[93] S. Plugge, A. Zazunov, E. Eriksson, A. Tsvelik, and R. Egger, "Kondo physics from quasiparticle poisoning in majorana devices," *arXiv preprint arXiv:1601.04332*, 2016.

[94] L. Fu, "Electron teleportation via Majorana bound states in a mesoscopic superconductor," *Physical review letters*, vol. 104, no. 5, p. 056402, 2010.

[95] C. W. Beenakker, "Search for Majorana fermions in superconductors," *arXiv preprint arXiv:1112.1950*, 2011.

[96] E. Eriksson, A. Nava, C. Mora, and R. Egger, "Tunneling spectroscopy of majorana-kondo devices," *Physical Review B*, vol. 90, no. 24, p. 245417, 2014.

[97] J. Martinek, Y. Utsumi, H. Imamura, J. Barnaś, S. Maekawa, J. König, and G. Schön, "Kondo effect in quantum dots coupled to ferromagnetic leads," *Physical review letters*, vol. 91, no. 12, p. 127203, 2003.

[98] P. P. Baruselli, R. Requist, M. Fabrizio, and E. Tosatti, "Ferromagnetic Kondo effect in a triple quantum dot system," *Physical review letters*, vol. 111, no. 4, p. 047201, 2013.

[99] J. J. Sakurai, *Advanced quantum mechanics*. Pearson Education India, 1967.